Controlling interplay between weak localization and interface-roughness scattering of electrons in nonlinear transport within a superlattice

Po-Hsin Shih,[1] Danhong Huang,[2,*] Godfrey Gumbs,[1] Thi-Nga Do,[3] Christian P. Morath,[2] and Diana Maestas[2]
[1]Department of Physics and Astronomy, Hunter College of the City University of New York, 695 Park Avenue, New York, New York 10065, USA
[2]Air Force Research Laboratory, Space Vehicles Directorate, Kirtland Air Force Base, Albuquerque, New Mexico 87117, USA
[3]Department of Physics, National Cheng Kung University, Tainan 701, Taiwan, Republic of China

(Received 2 May 2024; revised 25 July 2024; accepted 29 July 2024; published 16 August 2024)

In this study, we have explored simultaneously two distinctive physical aspects of electron transport within a semiconductor superlattice subjected to both randomly distributed barrier scattering strengths and in-plane interface-roughness scattering of electrons within each barrier layer. To include interface-roughness scattering of electrons within a single barrier layer, we adopt the reduced Boltzmann transport equation to compute the nonequilibrium occupation function of electrons. In the presence of randomness within a superlattice, we apply a quantum-mechanical transfer-matrix approach for an electron wave to take into account all barrier-layer scattering within the superlattice. Consequently, the single-electron group velocity has been replaced by a mean group velocity assisted with a randomness-averaged transmission coefficient. For the interface-roughness scattering of electrons by each barrier layer, we numerically solve the reduced Boltzmann transport equation exactly and acquire the electrical current by another weighted average of obtained mean group velocities over the numerically calculated transient nonequilibrium occupation function of electrons from the reduced Boltzmann transport equation.

DOI: 10.1103/PhysRevB.110.085303

I. INTRODUCTION

Physically speaking, if the length of a superlattice (SL) is short enough, i.e., on the order of ∼100 nm or a mesoscopic scale, such that the electron wave function is able to keep its phase coherence after they suffer multiple scatterings within the whole superlattice structure, then electron waves traveling through different paths can interfere with each other, leading to quantum interference. Such a mesoscopic physics phenomenon plays a profound role in electron transport. This quantum-interference effect of electron waves has attracted a great deal of interest, e.g., universal conductance fluctuations, and furthermore it has been discussed extensively in the context of solid-state physics for a long time [1–6]. Since then, various electron devices, which rely on this quantum-interference mechanism, have been proposed [7,8], including high-speed, low-power dissipation and multifunctionality applications. Meanwhile, quantum interference has also attracted much attention from a technological point of view. In the presence of interface roughness within each thin barrier layer of a superlattice [9], the scattering strengths of these barrier layers become random for vertically moving electron waves, even though the superlattice period is still a constant. This gives rise to a so-called weak-localization phenomenon for electron transport along the direction of a superlattice. Hereafter, the localization phenomenon studied in this paper refers only to a weak-localization effect on electrons in their transport.

Technological advances in submicron physics have finally enabled experimentalists to fabricate nearly ideal one-dimensional (1D) quantum wires [10]. The physics connection between electrical conductance at zero temperature and transmission coefficients, as shown by the well-known Landauer formula [11], indicates that some experimentally measurable quantities can be adequately accounted for when a simple infinite 1D array of short-range scatterers is introduced. The discovery of quasicrystals [12] has stimulated strong interest in exploring the physical nature of quasiperiodic (e.g., Fibonacci and Thue-Morse) sequences [13] as well as commensurate-incommensurate low-dimensional systems [14]. Previous works on quasiperiodic sequences have included plasmon excitation [15], localization [16], neutron polarization [17], density of states [18], optical-phonon tunneling [19], nonlinear optical filters [20], optical absorption in a random superlattice [21], electric-field-induced localization [22], as well as defect-assisted tunneling [23]. Interestingly, the quasiperiodicity in an infinite chain gives rise to a self-similar structure in the transmission of electrons as a function of their incident kinetic energy. Mathematically speaking, the disorder (fully random) chain leads to the well-known Anderson localization only when the chain becomes infinitely long. For a short disorder chain, on the other hand, there is no complete localization, and only an incomplete localization appears. Technically, as the chain length practically exceeds a threshold value, e.g., the *localization length*, the electron transport behaves very close to that found when there exists a complete localization. Therefore, the transmission of a long chain with disorder is expected to be extremely small.

On the other hand, the vertical transport of electrons in SLs has also gotten a lot of attention because of the unique band

*Contact author: danhong.huang@us.mil

 ©2024 American Physical Society

structures of InAs/GaSb SLs, which has played an important role in third-generation infrared focal-plane arrays and photodiodes [24–33]. For imaging application, the performance of optoelectronic devices needs high vertical carrier mobilities for efficient transport based on diffusion usually and/or drift sometimes [34]. Unfortunately, vertical mobilities cannot be measured directly since their measurement involves nonstandard and indirect experimental techniques, e.g., the geometric magnetoresistance [35,36]. As a result, the vertical mobility can be extracted indirectly by using the curve fitting to both vertical and lateral magnetotransport measurements [37,38]. There exist a lot of reported research works on in-plane transport within quantum wells [39], but there is no comparable effort for SL transport [40], even though the theory for diffusive carrier transport in SLs was developed early by Mori and Ando [41], Dharssi and Butcher [42], and others [43,44]. As a result, most theoretical and experimental efforts to date are still limited to horizontal transport [45].

Very recently, Szmulowicz *et al.* [46] established an analytic formalism for calculating simultaneously low-temperature vertical and horizontal mobilities, and they applied it to the case of InAs/GaSb SLs. In their work, both the numerically computed band-structure and the semiclassical Boltzmann transport theory, along with the measured in-plane mobilities, are combined to extract the vertical carrier mobilities so as to control interface-roughness scattering for enhancing device performance and material transport characteristics. However, their theory still employed a phenomenological relaxation-time approximation for a steady-state linear transport of electrons in InAs/GaSb SLs driven by a weak dc electric field.

The physics of semiconductor SLs under a strong dc electric field $\mathcal{E}_0$ appears very rich and interesting due to the large number of parameters that can be controlled quite easily in experiments. For example, eBloch oscillations in doped SLs, resulting in a negative differential conductance as predicted by Esaki and Tsu [47], were reported by Sibille *et al.* [35] for samples at room and low temperatures. In this situation, the acquired tunable strong terahertz (THz) emitter is used for real-time active spectral imaging after its combination with a focal-plane detector array [48]. Meanwhile, studies on long-time average current under ac monochromatic [49] and bichromatic [50] electric fields have also been reported, in which conditions for the presence of dynamical localization [51–53] were shown either for a scattering-free system or within the relaxation-time approximation for elastic scattering of electrons. Conditions for generalized dynamical localization under ac electric fields were also revealed after a tight-binding band structure beyond the nearest-neighbor approximation was employed [53,54].

Most recently, Shih *et al.* [9] have proposed and solved exactly the reduced Boltzmann transport equation with the full inclusion of microscopic scattering of electrons by impurities, phonons, interface roughness, etc. [55]. In their theory, instead of applying a relaxation-time approximation to scattering of electrons in the Boltzmann transport equation [46], a first-principles quantum-kinetic model [55] was employed for studying accurately the full effects of interface roughness on transient nonlinear vertical transport of electrons in SLs. To cut down computation time for very complex and time-consuming numerical calculations, an effective 1D occupation function was proposed for nonequilibrium miniband electrons in their vertical SL transport subjected to both dominant forward and secondly backward scatterings by in-plane interface roughness. Such a quantum-kinetic theory enables evaluating accurately nonlinear dc current and field-dependent mobility for vertical transport of miniband electrons in a SL through extracting its long-time steady-state currents under a fixed dc field. In this work, they assumed that the width $\mathcal{W}_0$ of a SL miniband is large and the applied dc field amplitude $\mathcal{E}_0$ is moderately high, so that the condition $e\mathcal{E}_0 d < \mathcal{W}_0$ can be satisfied to avoid Wannier-Stark strong localization of electrons within SLs [56,57], where d refers to the spatial period of SL.

In our current work, by introducing random fluctuations to barrier-scattering strengths in a SL [16,58], we explore the weak-localization phenomenon in a miniband transport of electrons, and we quantify the rejection current from randomness in the system, demonstrating an exponential dependence of current on SL sample length. Meanwhile, by simultaneously including interface-roughness-induced in-plane scattering of electrons, we reveal the interplay of weak localization with interface-roughness in nonlinear electron transport within a semiconductor SL, as well as the intriguing dependence of localization length in vertical transport of electrons on applied DC-field strength and temperature.

The rest of the paper is organized as follows. In Sec. II, we describe the weak-localization effect in a SL with random barrier-scattering strengths for out-of-plane electron scatterings. In Sec. III, we introduce the reduced Boltzmann transport equation for in-plane interface-roughness scattering of electrons within a SL. Numerical results and their discussions are presented in Sec. IV to highlight the interplay between the effects of weak localization and interface-roughness scattering on nonlinear electron transport within a semiconductor SL. Meanwhile, we also reveal in Sec. IV the unique dependence of weak-localization length on SL sample length, random barrier scattering strengths, temperature, and applied DC-field strength. Finally, a brief summary is given in Sec. V along with some remarks.

II. WEAK LOCALIZATION IN A SUPERLATTICE WITH RANDOM BARRIER-SCATTERING STRENGTHS FOR VERTICAL SCATTERING OF ELECTRONS

As shown in Fig. 1, by assuming a thin barrier layer satisfying $L_\text{B}/L_\text{W} \ll 1$, where L_B and L_W stand for the thicknesses of a barrier and a well layer, respectively, the SL scattering potential $V_\text{s}(z)$ for a total number of $N+2$ thin barrier layers can be approximately written as a chain of δ-function scatters, yielding

$$V_\text{s}(z) = \sum_{j=0}^{N+1} f_j\, \delta(z - jd), \tag{1}$$

where d is the SL period, $\mathcal{L} = (N+1)\,d$ is the SL length, and f_j (in the unit of energy $\times$ length) represents the scattering strength of the jth barrier layer due to the presence of interface roughness.

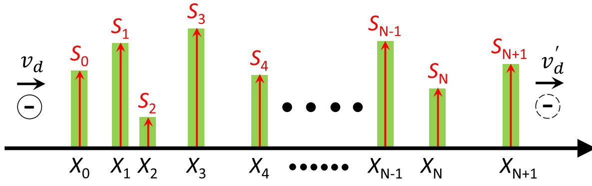

FIG. 1. Illustration of multiscatters of electrons inside a finite-length superlattice with $N+2$ potential barrier layers located at positions $\{X_0,\,X_1,\,X_2,\,\ldots,\,X_{N-1},\,X_N,\,X_{N+1}\}$, respectively, and having their corresponding randomly distributed scattering strengths $\{\mathcal{S}_0,\,\mathcal{S}_1,\,\mathcal{S}_2,\,\ldots,\,\mathcal{S}_{N-1},\,\mathcal{S}_N,\,\mathcal{S}_{N+1}\}$. Here, the drift velocity v_d for incoming electrons in this system will be changed to v_d' for outgoing ones due to successive barrier reflection of these moving electrons. For simplicity, only a periodic position arrangement for barrier layers will be considered, i.e., $x_j=(j-1)d$ for $j=1,\,2,\,\ldots,\,N+1,\,N+2$, where d is the superlattice period, but the random distribution of layer scattering strengths is retained.

As seen in Eq. (1), the effect of interface-roughness induced phase-sensitive vertical scattering of a single electron can be approximately described by a linear array of point-like scatters at these interface positions with their randomly selected scattering strengths $\{f_j\}$. For simplicity, we only assume two values for these randomly selected scattering strengths $f_j=\{s_1,\,s_2\}$. Importantly, this f_j value should not be confused with the SL barrier height V_0. In the present case, the scaled quantity, f_j/V_0d, becomes dimensionless and is usually assumed taking its values within a range between 0 and 0.5 [16].

Denoting $\psi_j^{(\mathrm{L,R})}(z)$ as electron wave functions on the left (L) and right (R) sides of the jth barrier layer, we find a relationship between them from the static Schrödinger equation including $V_s(z)$ in Eq. (1), i.e.,

$$\psi_j^{(\mathrm{R})}(z)=\hat{\mathcal{T}}_j(|k_z|)\,\psi_j^{(\mathrm{L})}(z), \tag{2}$$

where the transfer matrix $\hat{\mathcal{T}}_j(|k_z|)$ is given explicitly by [16,17]

$$\hat{\mathcal{T}}_j(|k_z|)=\begin{bmatrix}1-iq_j/2|k_z| & -iq_j/2|k_z|\\ iq_j/2|k_z| & 1+iq_j/2|k_z|\end{bmatrix}, \tag{3}$$

which is symmetric with respect to $\pm k_z$ as expected. In Eq. (3), $q_jd=2m_\parallel^* f_jd/\hbar^2$ is a dimensionless barrier-strength parameter, and $m_\parallel^*=2\hbar^2/\mathcal{W}_0d^2$ is the effective mass of electrons along the SL direction for the case of $|k_z|\ll\pi/d$. To see a significant dynamical effect in this system on electrons with low wave numbers k_z, $q_j/|k_z|\leqslant 1$ or $q_j\leqslant\pi/d$ is usually requested. Furthermore, two wave functions of an electron between the jth and $(j+1)$th barrier layers can be related to each other by

$$\psi_{j+1}^{(\mathrm{L})}(z)=\hat{\mathcal{D}}_j(|k_z|)\,\psi_j^{(\mathrm{R})}(z), \tag{4}$$

where the displacement matrix $\hat{\mathcal{D}}_j(|k_z|)$ takes the form

$$\hat{\mathcal{D}}_j(|k_z|)=\begin{bmatrix}\mathrm{e}^{i|k_z|d} & 0\\ 0 & \mathrm{e}^{-i|k_z|d}\end{bmatrix}. \tag{5}$$

By considering a weak localization due to fluctuated barrier strengths within a SL structure, the group velocity $v_z(k)=(1/\hbar)\,dE_z(k_z)/dk_z$ of a single electron should be replaced by an effective velocity $\overline{T}(|k_z|,\,\mathcal{L})\,v_z(k_z)$, where $E_z(k_z)=(\mathcal{W}_0/2)[1-\cos(k_zd)]$ for $|k_z|\leqslant\pi/d$ by using a tight-binding model, $\mathcal{W}_0$ is the bandwidth of an electron inside the SL, and $\overline{T}(|k_z|,\,\mathcal{L})$, as presented in Eq. (11) below, stands for an average transmission coefficient for an incident electron with its vertical wave number k_z throughout the whole SL between two electrodes. Consequently, the transient current for vertical transport of electrons through the SL takes the form [9]

$$\begin{aligned}I^{(\mathrm{loc})}(t,\,\mathcal{L}\,|\,\mathcal{E}_0)&=\frac{e}{\pi}\int_{-\pi/d}^{\pi/d}dk_z\,\overline{v}_z(k_z)\,\Delta n(k_z,t)\\&=\frac{e}{\pi}\int_{-\pi/d}^{\pi/d}dk_z\,\overline{T}(|k_z|,\,\mathcal{L})\,v_z(k_z)\,\Delta n(k_z,t)\\&=\frac{e\mathcal{W}_0d}{2\pi\hbar}\int_{-\pi/d}^{\pi/d}dk_z\,\overline{T}(|k_z|,\,\mathcal{L})\\&\quad\times\sin(k_zd)\,\Delta n(k_z,t),\end{aligned} \tag{6}$$

where $v_z(k_z)$ is a group velocity of electrons in the absence of localization, while $\overline{v}_z(k_z)\equiv\overline{T}(|k_z|,\,\mathcal{L})\,v_z(k_z)$ represents an effective group velocity of electrons in the presence of weak localization. Additionally, $\Delta n(k_z,t)$ is the nonequilibrium part of the full electron occupation function under a dc field, which will be calculated and discussed in Sec. III below. Furthermore, the individual transmission coefficient $T(k_z)$ for any given SL barrier configuration can be calculated [16,58] by a total transfer matrix involving a product of many transfer and displacement matrices for randomly fluctuated barrier scattering strengths. From Eq. (6), we know that the current reduction (or rejection current) $I^{(\mathrm{rej})}(t\,|\,\mathcal{E}_0)$ is

$$\begin{aligned}I^{(\mathrm{rej})}(t,\,\mathcal{L}\,|\,\mathcal{E}_0)&=\frac{e}{\pi}\int_{-\pi/d}^{\pi/d}dk_z\,[1-\overline{T}(|k_z|,\,\mathcal{L})]v_z(k_z)\Delta n(k_z,t)\\&=\frac{e\mathcal{W}_0d}{2\pi\hbar}\int_{-\pi/d}^{\pi/d}dk_z\,\overline{R}(|k_z|,\,\mathcal{L})\\&\quad\times\sin(k_zd)\,\Delta n(k_z,t),\end{aligned} \tag{7}$$

which increases with the SL sample length $\mathcal{L}$ exponentially, where $\overline{R}(|k_z|,\,\mathcal{L})=1-\overline{T}(|k_z|,\,\mathcal{L})$ is the average reflection coefficient for an incident electron with a vertical wave number k_z.

By making use of the layer-index specified transfer and displacement matrices in Eqs. (3) and (5), the total transfer matrix $\hat{\mathcal{M}}_{\mathrm{tot}}(|k_z|)$, relating the first $(j=0)$ to the last $(j=N+1)$ barrier layer, can be expressed as

$$\begin{aligned}\hat{\mathcal{M}}_{\mathrm{tot}}(|k_z|)&=\{\hat{\mathcal{T}}_{N+1}(|k_z|)\}\otimes\{\hat{\mathcal{D}}_N(|k_z|)\,\hat{\mathcal{T}}_N(|k_z|)\}\\&\quad\otimes\cdots\otimes\{\hat{\mathcal{D}}_0(|k_z|)\,\hat{\mathcal{T}}_0(|k_z|)\}\\&\equiv\begin{bmatrix}\mathcal{M}_{11}(|k_z|) & \mathcal{M}_{12}(|k_z|)\\ \mathcal{M}_{21}(|k_z|) & \mathcal{M}_{22}(|k_z|)\end{bmatrix}\\&=\begin{bmatrix}1/t^*(|k_z|) & -r^*(|k_z|)/t^*(|k_z|)\\ -r(|k_z|)/t(|k_z|) & 1/t(|k_z|)\end{bmatrix},\end{aligned} \tag{8}$$

where $t(|k_z|)$ and $r(|k_z|)$ are two complex amplitudes for forward- and backward-going wave functions: $\mathcal{M}_{22}(|k_z|)=\mathcal{M}_{11}^*(|k_z|)=1/t(|k_z|)$ and $\mathcal{M}_{21}(|k_z|)=\mathcal{M}_{12}^*(|k_z|)=-r(|k_z|)/t(|k_z|)$. As a result, the total

transmission $T(|k_z|,\ \mathcal{L})$ and reflection $R(|k_z|,\ \mathcal{L})$ coefficients for a SL can be evaluated from

$$T(|k_z|,\ \mathcal{L}) = |t(|k_z|,\ \mathcal{L})|^2 = \frac{1}{|\mathcal{M}_{22}(|k_z|)|^2}, \tag{9}$$

$$R(|k_z|,\ \mathcal{L}) = |r(|k_z|,\ \mathcal{L})|^2 = 1 - T(|k_z|,\ \mathcal{L}) = \frac{|\mathcal{M}_{21}(|k_z|)|^2}{|\mathcal{M}_{22}(|k_z|)|^2}. \tag{10}$$

To simulate randomness in barrier scattering strengths of a SL system, we assume that the barrier scattering strength, $q_j d/\pi \leqslant 1/2$ for $j = 0,\ 1,\ \ldots,\ (N+1)$, only takes one of two values, s_1 and s_2, each time in a random way with $s_1 \neq s_2 \in [0,\ 0.5]$. Therefore, for any given sequence $\{q_j\} \equiv (q_0,\ q_1,\ q_2,\ \ldots,\ q_{N-2},\ q_{N+1})_{q_j\in\{s_1,s_2\}}$ within the range of $[0,\ 0.5]$, in a relation to randomly distributed barrier scattering strengths of different barrier layers, we are able to calculate its transmission coefficient $T(|k_z|\,|\,q_j \in \{s_1, s_2\},\ 0 \leqslant j \leqslant N+1)$ from Eqs. (8)–(10). Consequently, the average transmission coefficient $\overline{T}(|k_z|,\ \mathcal{L})$ employed in Eq. (6) can be calculated from

$$\overline{T}(|k_z|,\ \mathcal{L}) = \frac{1}{\mathcal{M}_0}\sum_{\{q_j\}=1}^{\mathcal{M}_0} T(|k_z|,\ q_j \in \{s_1, s_2\},\ 0 \leqslant j \leqslant N+1), \tag{11}$$

where we have selected totally $\mathcal{M}_0$ ($\gg 1$) independent configurations of random sequence $\{q_j\}$ with $q_j \in \{s_1, s_2\}$ and $0 \leqslant j \leqslant N+1$ for a distribution of barrier scattering strengths in this averaging process.

From Eq. (11) we know that $\overline{T}(|k_z|,\ \mathcal{L})$ is a function of k_z and also depends on SL length $\mathcal{L}$ and randomness parameters $\{q_j\}$. However, $\overline{T}(|k_z|,\ \mathcal{L})$ will not rely on dc field $\mathcal{E}_0$. By including the weak-localization (or transient carrier trapping) effect, we find from Eq. (6) that the current $I^{(\text{loc})}(t,\ \mathcal{L}\,|\,\mathcal{E}_0)$ not only changes with $\mathcal{L}$ and $\{q_j\}$ but also relies on $\mathcal{E}_0$ due to its connection to the $\mathcal{E}_0$-dependent nonequilibrium occupation $\Delta n(k_z, t)$. Meanwhile, as expected from Eq. (6), the transient localization current $I^{(\text{loc})}(t,\ \mathcal{L}\,|\,\mathcal{E}_0)$ can alter its magnitude with various selections of $\mathcal{L}$ and $\{q_j\}$. For the steady-state current $I^{(\text{loc})}(t,\ \mathcal{L}\,|\,\mathcal{E}_0)$, on the other hand, it will also depend on $\mathcal{L}$ and $\{q_j\}$ due to the weak localization of electrons in addition to the fact that $I^{(\text{loc})}(t,\ \mathcal{L}\,|\,\mathcal{E}_0)$ appears as functions of both $\mathcal{E}_0$ and temperature T, which reveals the weak-localization contribution to the resistance characteristics of the system.

Equation (6) can be employed generally to calculate a steady-state current flowing through a SL system under a dc electric field $\mathcal{E}_0$. Substituting $\overline{T}(|k_z|,\ \mathcal{L})$ formulated in Eq. (11) for the effect of random barrier scattering strength into Eq. (6) in this SL system, we are able to obtain a transient current $I^{(\text{loc})}(t,\ \mathcal{L}\,|\,\mathcal{E}_0)$, which includes weak-localization effects. Furthermore, we can formally define a steady-state current in the form of $I^{(\text{loc})}(\mathcal{L}\,|\,\mathcal{E}_0) = I_0(\mathcal{E}_0)\exp(-\mathcal{L}/\xi_{\text{loc}})$ as $t \to \infty$, where $I_0(\mathcal{E}_0)$ represents the corresponding current in the absence of localization, or equivalently as $\xi_{\text{loc}}(\mathcal{L}\,|\,\mathcal{E}_0) \gg \mathcal{L}$. Therefore, the localization length $\xi_{\text{loc}}(\mathcal{L}\,|\,\mathcal{E}_0)$ can be written simply as

$$\xi_{\text{loc}}(\mathcal{L}\,|\,\mathcal{E}_0) = -\lim_{t\to\infty}\frac{\mathcal{L}}{\ln[I^{(\text{loc})}(t,\ \mathcal{L}\,|\,\mathcal{E}_0)/I_0(t,\ \mathcal{E}_0)]}, \tag{12}$$

where $\mathcal{L} = (N+1)\,d$ stands for the SL length. Moreover, $I_0(t,\ \mathcal{E}_0)$ in Eq. (12) can be calculated from Eq. (6) under the condition of $\overline{T}(|k_z|,\ \mathcal{L}) \equiv 1$. The unique dependence on $\mathcal{L}$ in Eq. (12) for $I^{(\text{loc})}(t,\ \mathcal{L}\,|\,\mathcal{E}_0) < I_0(t,\ \mathcal{E}_0)$ implies an incomplete localization phenomenon for steady-state electrons within a finite-length SL system, which eventually turns into a full-localization system as $\mathcal{L} \longrightarrow \infty$ with a negligible current.

Additionally, one finds from Eq. (6) that the electrical current flowing through a SL also depends on the interplay between the average transmission coefficient $\overline{T}(|k_z|,\ \mathcal{L})$ and the nonequilibrium occupation function $\Delta n(k_z, t)$, where the former describes a vertical-scattering facilitated weak-localization effect on moving electrons due to the presence of randomly distributed barrier scattering strengths while the latter determines an in-plane scattering effect on electrons due to the existence of interface roughness within the SL structure. Here, the randomness in SL is quantified by the selection of s_1 and s_2 values for the random barrier-strength parameter q_j for out-of-plane scattering of electrons. The interface-roughness scattering, however, is measured by its effective 1D scattering potentials presented in Eqs. (B1) and (B2) for in-plane scattering of electrons, which relies on externally applied dc field amplitude $\mathcal{E}_0$ and temperature T and is determined from the reduced Boltzmann transport equation discussed in Sec. III.

Our previous paper [9] has demonstrated an effective approach for accurate computation of the effect of parallel interface-roughness scattering on electron transport within a superlattice structure. In this work, on the other hand, we propose a new concept and research related to unique dynamics for the combination and competition of distinctive in-plane and out-of-plane scattering mechanisms within the same superlattice system. As seen in Eq. (6), in the presence of a localization effect on transport electrons, an accurate calculation of vertical electrical current requires a single-electron transmission coefficient $\overline{T}(|k_z|, \mathcal{L})$ for an averaged group velocity of Bloch electrons as well as a nonequilibrium distribution function $\Delta n(k_z, t)$ for bias-field driven electrons by solving a semiclassical Boltzmann equation [9]. On the contrary, previous theories on localization of superlattice electrons often replace $\Delta n(k_z, t)$ by a difference between two thermal-equilibrium distribution functions of electrons in a left and right electrical contact, respectively, with a fixed voltage drop between them [59].

From a physics perspective, the current work includes simultaneously both out-of-plane and in-plane random scatterings of transport electrons within the same superlattice, and their interplay as well. As a result, distinctive dynamics and effects, associated with either multistep scatterings of a single electron with a series of rough barrier layers along the perpendicular (superlattice) direction or many single-step scatterings of different electrons by the same rough interface in the parallel (interface) direction, have been mixed together by a vertical transport of electrons, leading to a new dynamics for vertical electron transport within a superlattice, such as unique temperature, bias-field strength, and

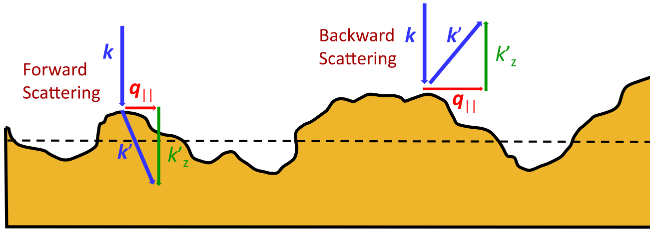

FIG. 2. Illustrations for forwarded scattering ($k_z'>0$) and backward scattering ($k_z'<0$) by roughness (solid black curve) on one interface (black dashed line) within a SL, where $q_z=k_z'-k_z$, $\boldsymbol{q}_\parallel=\boldsymbol{k}_\parallel'-\boldsymbol{k}_\parallel$ are transition wave numbers, and the total kinetic energy of electrons must be conserved for these elastic-scattering events. Moreover, one must replace k_z' by $k_z'\pm 2\pi/d$ to maintain $|k_z'|\leqslant\pi/d$ within the first Brillouin zone once $|k_z'|>\pi/d$ for the umklapp scattering.

interface-roughness scattering dependence in a localization length for electron transport in a superlattice.

III. REDUCED BOLTZMANN EQUATION FOR VERTICAL TRANSPORT WITH IN-PLANE ROUGHNESS SCATTERING IN A SUPERLATTICE

As seen in Eq. (6), the vertical electron transport current $I^{(\mathrm{loc})}(t,\,\mathcal{L}\,|\,\mathcal{E}_0)$, including the weak-localization effect from vertical random scattering of electrons, also depends on the nonequilibrium occupation function $\Delta n(k_z,\,t)$. As explained in Fig. 2, $\Delta n(k_z,\,t)$ results from the in-plane scattering of electrons in the presence of interface roughness. We would like to point out that the inclusion of $\Delta n(k_z,\,t)$ in Eq. (6) allows one to bring field and thermal effects into consideration for a localized electrical current. Thereafter, we present the computation and discussion of $\Delta n(k_z,\,t)$.

From the discussions in Appendix A, we are able to project Eq. (A1) directly onto a 1D k_z-space ($|k_z|\leqslant\pi/d$) and acquire the following reduced Boltzmann transport equation:

$$\frac{d}{dt}\Delta n(k_z,t)=\left.\frac{\partial n(k_z,t)}{\partial t}\right|_{\mathrm{scat}}-\frac{\mathcal{F}(t)}{\hbar}\left[\frac{\partial n_0(k_z)}{\partial k_z}+\frac{\partial\Delta n(k_z,t)}{\partial k_z}\right],\tag{13}$$

where $\Delta n(k_z,t)\equiv n(k_z,t)-n_0(k_z)$, which is zero at $t=0$, and $n_0(k_z)$ is the initial thermal-equilibrium distribution of electrons given in Eq. (22). Therefore, $\Delta n(k_z,t)$ represents only the nonequilibrium part of the full electron distribution. Equation (13) can be utilized to evaluate the time-dependent nonequilibrium distribution $\Delta n(k_z,t+\Delta t)$ for $|k_z|<\pi/d$ based on a so-called three-point central-difference formula [60] for the drifting term $\partial\Delta n(k_z,t)/\partial k_z$ and known values for $\Delta n(k_z,t)$ at an early time t. However, the values of $n(k_z=\pm\pi/d,t+\Delta t)$ should still be determined by the periodic condition $n(k_z=\pi/d,t+\Delta t)=n(k_z=-\pi/d,t+\Delta t)$ as well as the restraint for conservation of the total number of doped electrons within the superlattice [60]. This yields

$$\frac{d}{2\pi}\int_{-\pi/d}^{\pi/d}dk_z\,\Delta n(k_z,t+\Delta t)\equiv 0.\tag{14}$$

Consequently, we expect that $\Delta n(k_z=\pm\pi/d,t+\Delta t)$ at two boundary points can be determined from $\Delta n(k_z,t+\Delta t)$ within the range of $|k_z|<\pi/d$, leading to

$$g_1(t+\Delta t)=g_M(t+\Delta t)=-\frac{1}{2}\sum_{j=2}^{M-1}g_j(t+\Delta t),\tag{15}$$

from which we easily find

$$\sum_{j=1}^{M}g_j(t+\Delta t)\equiv 0,\tag{16}$$

where $g_j(t+\Delta t)\equiv\Delta n(k_j,t+\Delta t)$ for $1\leqslant j\leqslant M$, $k_j=-\pi/d+(j-1)\Delta k$, $\Delta k=2\pi/(M-1)d$, and $M\geqslant 3$ is an integer representing a total number of equal-distance discrete points within the range of $|k_z|\leqslant\pi/d$. Here, we emphasize that our calculated $\Delta n(k_z,t)$ from Eq. (13) will show $\Delta n(k_z,t)\neq\Delta n(-k_z,t)$ for $|k_z|<\pi/d$ if a finite bias field is applied, although $\Delta n(k_z=\pi/d,t)=\Delta n(k_z=-\pi/d,t)$ is still maintained.

Furthermore, we have introduced in Eq. (13) a reduced Boltzmann-type scattering term on its right-hand side, which is given explicitly by

$$\begin{aligned}\left.\frac{\partial n(k_z,t)}{\partial t}\right|_{\mathrm{scat}}&\approx\frac{2}{n_{\mathrm{qw}}\mathcal{A}}\sum_{\mathbf{k}_\parallel}\left.\frac{\partial f(\{\boldsymbol{k}_\parallel,\,k_z\},\,t)}{\partial t}\right|_{\mathrm{scat}}^{(\mathrm{in})}[1-f_0(E_{xy}(k_\parallel)-\mu_0)]-\frac{2}{n_{\mathrm{qw}}\mathcal{A}}\sum_{\mathbf{k}_\parallel}\left.\frac{\partial f(\{\boldsymbol{k}_\parallel,\,k_z\},\,t)}{\partial t}\right|_{\mathrm{scat}}^{(\mathrm{out})}f_0(E_{xy}(k_\parallel)-\mu_0)\\&\equiv\mathcal{W}_{\mathrm{in}}(k_z,t\,|\,n_0+\Delta n)[1-n_0(k_z)-\Delta n(k_z,t)]-\mathcal{W}_{\mathrm{out}}(k_z,t\,|\,n_0+\Delta n)[n_0(k_z)+\Delta n(k_z,t)]\\&\quad-\delta_{t,0}\left[\mathcal{W}_{\mathrm{in}}^{(0)}(k_z\,|\,n_0)[1-n_0(k_z)]+\mathcal{W}_{\mathrm{out}}^{(0)}(k_z\,|\,n_0)\,n_0(k_z)\right],\end{aligned}\tag{17}$$

where the detailed-balance condition has been employed for the initial state $n(k_z,t=0)$. From discussions in Appendix B, we write down the reduced 1D scattering-in and scattering-out rates employed in Eq. (17) as

$$\begin{aligned}\mathcal{W}_{\mathrm{in}}(k_z,t\,|\,n_0+\Delta n)&\approx\frac{2}{n_{\mathrm{qw}}\mathcal{A}}\sum_{\mathbf{k}_\parallel}W_{\mathrm{in}}(\boldsymbol{k},t\,|\,f)\,[1-f_0[E_{xy}(k_\parallel)-\mu_0]]\equiv\frac{2\pi}{\hbar}\sum_{k_z'}U_{\mathrm{sc}}^{(\mathrm{in})}(k_z,k_z')[n_0(k_z')+\Delta n(k_z',t)]\\&=\frac{U_{\max}\,d}{\hbar}\int_{-\pi/d}^{\pi/d}dk_z'\,\overline{U}_{\mathrm{sc}}^{(\mathrm{in})}(k_z,k_z')[n_0(k_z')+\Delta n(k_z',t)],\end{aligned}\tag{18}$$

$$\mathcal{W}_{\rm out}(k_z,t\,|\,n_0+\Delta n)\approx\frac{2}{n_{\rm qw}\mathcal{A}}\sum_{\mathbf{k}_\|}W_{\rm out}(\boldsymbol{k},t\,|\,f)\,f_0[E_{xy}(k_\|)-\mu_0]\equiv\frac{2\pi}{\hbar}\sum_{k_z'}U_{\rm sc}^{(\rm out)}(k_z,k_z')[1-n_0(k_z')-\Delta n(k_z',t)]$$
$$=\frac{U_{\max}\,d}{\hbar}\int_{-\pi/d}^{\pi/d}dk_z'\,\overline{U}_{\rm sc}^{(\rm out)}(k_z,k_z')\,[1-n_0(k_z')-\Delta n(k_z',t)]. \tag{19}$$

Here, $\mathcal{W}_{\rm in}^{(0)}(k_z\,|\,n_0)$ and $\mathcal{W}_{\rm out}^{(0)}(k_z\,|\,n_0)$ in Eq. (17) can be easily obtained from Eqs. (18) and (19) after setting $\Delta n=0$. Moreover, we have assumed a thermal-equilibrium distribution $f_0[E_{xy}(k_\|)-\mu_0]=(1+\exp\{[E_{xy}(k_\|)-\mu_0(T)]/k_BT\})^{-1}$ in Eq. (17) for in-plane roughness-scattering motions, which has been used in Eqs. (B1) and (B2) and reduces to $\Theta(E_F-E_{xy}(k_\|))$ with the Fermi energy E_F at low temperatures $k_BT\ll E_F$, where $E_{xy}(k_\|)=\hbar\Omega_0/2+\hbar^2k_\|^2/2m^*$. In Eqs. (18) and (19), we define $\overline{U}_{\rm sc}(k_z,k_z')\equiv U_{\rm sc}(k_z,k_z')/U_{\max}$ with a maximum value $U_{\max}$ for $|U_{\rm sc}(k_z,k_z')|$, and we assume that $\Delta t\ll U_{\max}/\hbar$. In fact, Eq. (17) becomes nonlinear with respect to $\Delta n(k_z,t)$ since $\mathcal{W}_{\rm in}$ and $\mathcal{W}_{\rm out}$ themselves depend on $n(k_z,t)$.

Meanwhile, the effective 1D inverse energy-relaxation time is calculated as

$$\frac{1}{\tau_1(k_z)}=\frac{2}{n_{\rm qw}\mathcal{A}}\sum_{\mathbf{k}_\|}\frac{1}{\tau_{\rm E}(\boldsymbol{k})}\approx\frac{2\pi}{\hbar}\sum_{k_z'}\Big\{U_{\rm sc}^{(\rm out)}(k_z,k_z')+\big[U_{\rm sc}^{(\rm in)}(k_z,k_z')-U_{\rm sc}^{(\rm out)}(k_z,k_z')\big]\,n(k_z',t)\Big\}, \tag{20}$$

which also depends on $n(k_z',t)$. The quantum-statistical average of this effective 1D inverse energy-relaxation time further leads to

$$\frac{1}{\tau_0(t)}=\frac{d}{2\pi}\int_{-\pi/d}^{\pi/d}dk_z\,[n_0(k_z)+\Delta n(k_z,t)]\,\frac{1}{\tau_1(k_z)}. \tag{21}$$

Here, $\tau_0(t)$ in Eq. (21) can be regarded as a macroscopic energy-relaxation time, which is often used in the so-called relaxation-time approximation and relates to the random interface-roughness scattering within the SL system.

On the left-hand side of Eq. (13), we have introduced a time-dependent force $\mathcal{F}(t)$ pointing towards the SL (z) direction, which is given by

$$\mathcal{F}(t)=-\frac{e\mathcal{E}_0}{M}\sum_{j=1}^{M}\left[\frac{1}{2}+\frac{1}{\pi}\,\tan^{-1}\left(\frac{t-j\Delta t}{\delta_0}\right)\right],$$

where M stands for the total number of turning-on steps, $\mathcal{E}_0$ ($e\mathcal{E}_0d<\mathcal{W}_0$) is the magnitude of an applied dc field, $t_j=j\Delta t$ is the jth turning-on time, Δt is the waiting (or stage) time, and δ_0 ($\ll\Delta t$) represents the broadening for a turning-on time at $t=t_j$.

Since the dc field is applied after $t=0$, the initial condition for occupation function $n(k_z,t)$ at $t=0$ can be simply set as a thermal-equilibrium Fermi function at temperature T, yielding

$$n(k_z,t=0)=n_0(k_z)$$
$$=\frac{2}{n_{\rm qw}\mathcal{A}}\sum_{\mathbf{k}_\|}\left\{1+\exp\left[\frac{\varepsilon_{\mathbf{k}_\|,k_z}-\mu_0(T)}{k_BT}\right]\right\}^{-1}$$
$$=\frac{1}{\pi n_{\rm qw}}\int_0^\infty dk_\|\,k_\|\left\{1+\exp\left[\frac{\varepsilon_{\mathbf{k}_\|,k_z}-\mu_0(T)}{k_BT}\right]\right\}^{-1}, \tag{22}$$

where $\mu_0(T)$ is the chemical potential, which, for a given volume doping density ρ_0, is determined by the root of a constraint equation [61] for any fixed value of T, i.e.,

$$\rho_0=\frac{1}{2\pi^2}\int_{-\pi/d}^{\pi/d}dk_z\int_0^\infty dk_\|\,k_\|\times\left\{1+\exp\left[\frac{\varepsilon_{\mathbf{k}_\|,k_z}-\mu_0(T)}{k_BT}\right]\right\}^{-1}, \tag{23}$$

where $\varepsilon_{\mathbf{k}_\|,k_z}=E_{xy}(k_\|)+E_z(k_z)$ with their expressions given in Appendix B. With this determined chemical potential $\mu_0(T)$, we further obtain the quantum-well areal density $n_{\rm qw}\approx\rho_0d$ of electrons used in Eq. (22).

It is well known that both the nonequilibrium Green's function [62] (NEGF) and the Wigner equation [63] are quantum theories, which, in particular, can be applied to find coherent (and tunneling) transport of electrons in the presence of one or more static or transient potential barriers on the transport path of electrons. However, both of them usually do not treat exactly nonlocal dynamics associated with random pair, phonon, roughness, and impurity scatterings of carriers. Instead, only a simple and finite lifetime parameter will be introduced sometimes to account for the scattering effect of electrons.

On the other hand, the Boltzmann transport equation employed in this work is a semiclassical theory, and we have solved it exactly after having fully considered nonlocal random scattering of electrons with interface roughness within a superlattice beyond the commonly used relaxation-time approximation and a linearized Boltzmann transport equation [60]. In fact, the calculated nonlinear dependence on a bias-field strength in electrical current (i.e., so called non-Ohmic behavior under a high bias field) results directly from random interface-roughness scattering of electrons in a superlattice. Here, the presence of periodic barrier layers within a superlattice structure has been taken into account directly by using a tight-binding band structure for Bloch electrons.

Furthermore, the localization effect originates from an average over multiple scatterings of a single electron with many barrier layers with fluctuated strengths along the perpendicular (superlattice) direction. On the other hand, the interface-scattering effect results from a different average over many one-time collisions of various electrons with the same

TABLE I. Parameters used for numerical calculations of electron transport in a superlattice.

Parameter	Description	Value	Unit
$\hbar\Omega_0$	energy-level separation	100	meV
$\mathcal{W}_0$	miniband width	10	meV
$N+1$	number of SL periods	51	unitless
d	SL period	100	Å
ρ_0	electron volume density	1	10^{16} cm^{-3}
m^*	in-plane electron effective mass	0.067	9.1×10^{-31} kg
Γ_0	electron lifetime broadening	0.5	meV
Δ_0	average interface roughness	5	Å
Λ_0	in-plane correlation length	30	Å
M	number of time steps	5	unitless
Δt	waiting time	10	ps
$\mathcal{M}_0$	number of random configurations	1000	unitless
δ_0	broadening time	0.5	ps
$\tilde{\mathcal{E}}_0$	DC electric field	0.5	kV/cm
T	temperature	4 (77)	K

rough interface in the parallel (interface) direction. Clearly, the unique combination of these two distinctive scattering mechanisms in the same system is not only novel and unique in physics but also very important for device applications and increasing its performance limit.

IV. NUMERICAL RESULTS AND DISCUSSIONS

The used parameters in our numerical computations are listed in Table I. The parameters that are not given in Table I will be provided directly in individual figure captions.

A. Effect of random barrier strength on electron transmission

As seen in Fig. 3, for $N = 50$, $s_1 = 0.01$, and fixed SL length $\mathcal{L} = (N+1)\,d$ (left panel), we observe that the computed average electron transmission coefficient $\overline{T}(|k_z|,\ \mathcal{L})$ becomes zero around $k_z = 0$ by displaying a "gap," but it approaches unity around $k_z = \pm\pi/d$, appearing as a "hall way." On the other hand, as s_2 value increases gradually from 0.002 up to 0.02 by an order of magnitude for fixed $s_1 = 0.01$, $\overline{T}(|k_z|,\ \mathcal{L})$ first increases and then deceases away from $k_z = 0$. In particular, $\overline{T}(|k_z|,\ \mathcal{L})$ approach unity as s_2 becomes close to given $s_1 = 0.01$ because of reduced randomness or the weak-localization effect within the SL system. For $s_1 = 0.01$ and $s_2 = 0.005$ (right panel), $\overline{T}(|k_z|,\ \mathcal{L})$ decreases with increasing N from 50 to 500 due to inclusion of more vertical-scattering layers for random fluctuations, leading to enhanced randomness or weak localization in this system. Very interestingly, we find that $\overline{T}(|k_z|,\ \mathcal{L}) < 1/2$ while $\overline{R}(|k_z|,\ \mathcal{L}) > 1/2$ in the region around $k_z = 0$. For the other two regions close to $k_z = \pm\pi/d$, on the other hand, the opposite feature is observed.

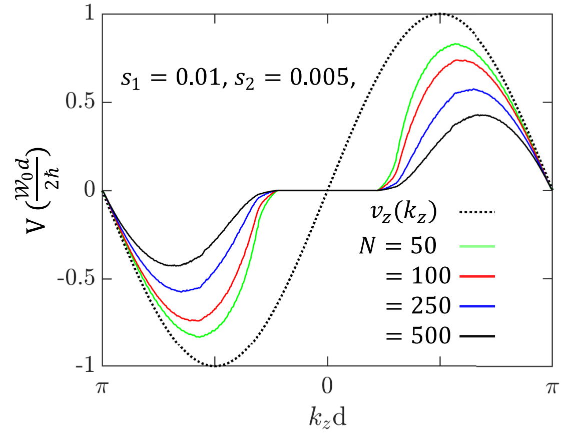

FIG. 4. Comparison for the computed average group velocity $\overline{v}_z(k_z,\ \mathcal{L}) = \overline{T}(|k_z|,\ \mathcal{L})\,v_z(k_z)$ as a function of k_z for $s_1 = 0.01$, $s_2 = 0.005$, and various N values. The dotted curve corresponds to the case without randomness or $\overline{T}(|k_z|,\ \mathcal{L}) \equiv 1$.

B. Dependence of electron tunneling current on random barrier scattering strength, dc field, and sample length

When the randomness effect in the system has been ignored, i.e., $s_1 = s_2$, one arrives at $\overline{T}(|k_z|,\ \mathcal{L}) \equiv 1$ corresponding to a perfect transmission in a SL for all k_z values, and then $\overline{v}_z(k_z,\ \mathcal{L})$ reduces to $v_z(k_z) = (1/\hbar)\,dE_z(k_z)/dk_z$, as presented by the black dotted curve in Fig. 4. As $s_1 = 0.01$ and $s_2 = 0.005$ are taken, on the other hand, the weak-localization

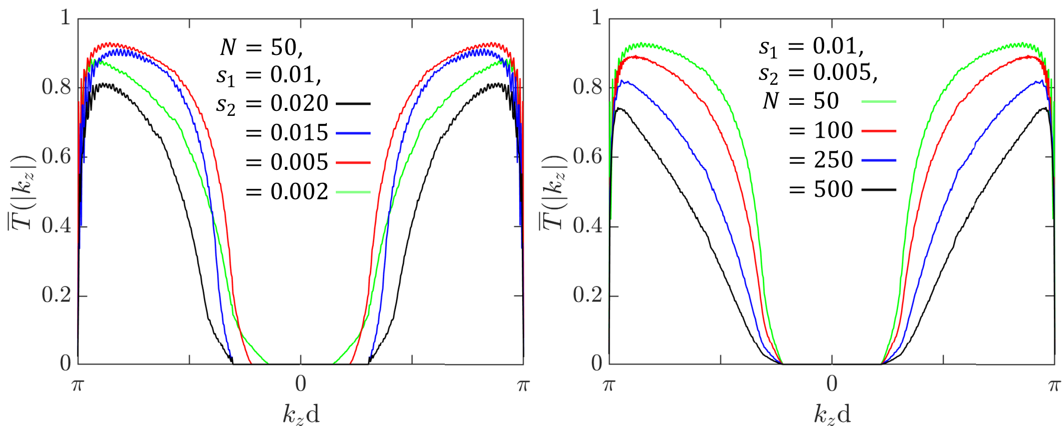

FIG. 3. Calculated average electron transmission coefficient $\overline{T}(|k_z|,\ \mathcal{L})$ as a function of electron wave number k_z for $N = 50$ and scattering strengths $s_1 = 0.01$ but different s_2 values (left), as well as for $s_1 = 0.01$, $s_2 = 0.005$, but various selections of N values (right).

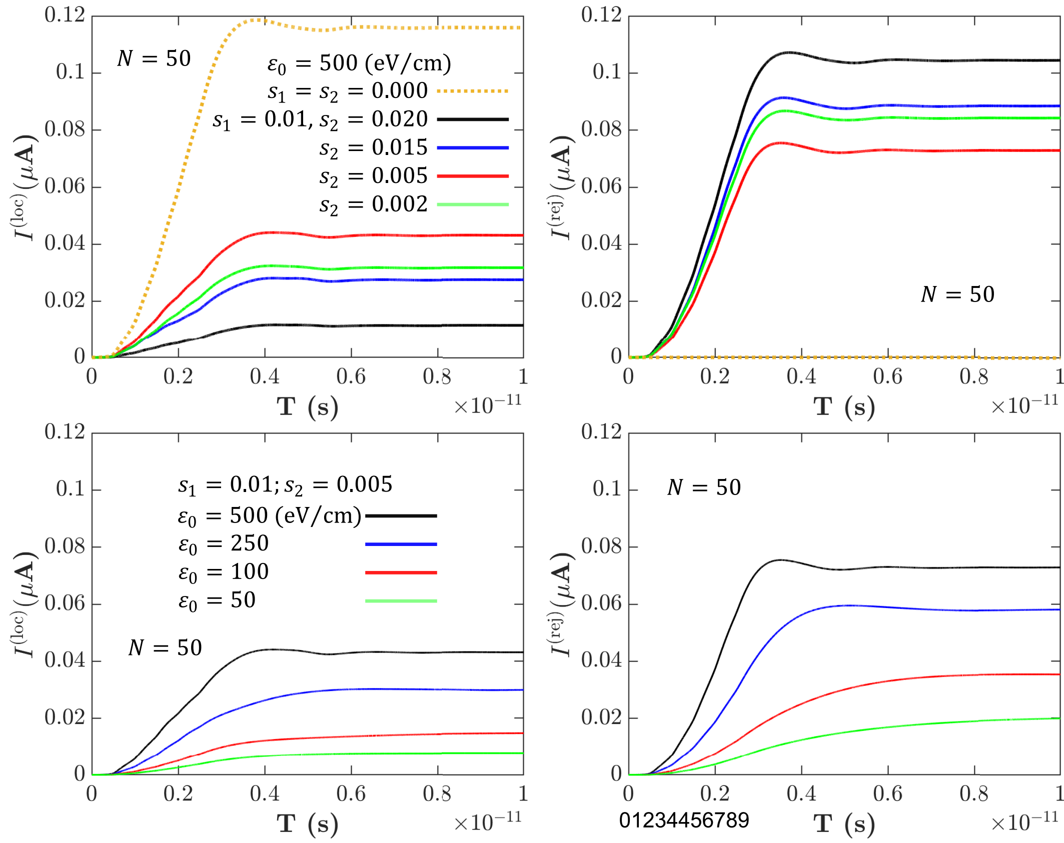

FIG. 5. Plots for forward $I^{(\mathrm{loc})}(t,\ \mathcal{L}\,|\,\mathcal{E}_0)$ (left) and backward $I^{(\mathrm{rej})}(t,\ \mathcal{L}\,|\,\mathcal{E}_0)$ (right) electrical currents at $T = 4$ K as a function of time t with $N = 50$, $\mathcal{E}_0 = \tilde{\mathcal{E}}_0$ for various values of $s_1,\ s_2$ (upper row) as well as for $s_1 = 0.01$ and $s_2 = 0.005$ but different values of $\mathcal{E}_0$ (lower row).

effect has been brought into the SL system due to the presence of randomness. Particularly, as N increases gradually from 50 to 500, the black dotted curve for $v_z(k_z)$ is deformed by a full suppression of $\overline{v}_z(k_z,\ \mathcal{L})$ to zero within a region around $k_z = 0$, corresponding to the observation of a "gap" for $\overline{T}(|k_z|,\ \mathcal{L})$ in Fig. 3. Meanwhile, the bowl-shaped $\overline{v}_z(k_z,\ \mathcal{L})$ outside this gap region decreases with increasing N value due to enhanced randomness or the weak-localization effect in the system, similar to the observation of $\overline{T}(|k_z|,\ \mathcal{L})$ in the right panel of Fig. 3.

The calculations of forward $I^{(\mathrm{loc})}(t,\ \mathcal{L}\,|\,\mathcal{E}_0)$ and backward $I^{(\mathrm{rej})}(t,\ \mathcal{L}\,|\,\mathcal{E}_0)$ currents in the SL system are given in Eqs. (6) and (7), respectively. Here, in spite of the fact that both $I^{(\mathrm{loc})}(t,\ \mathcal{L}\,|\,\mathcal{E}_0)$ and $I^{(\mathrm{rej})}(t,\ \mathcal{L}\,|\,\mathcal{E}_0)$ depend on $\overline{T}(|k_z|,\ \mathcal{L})$, $I_0(t,\ \mathcal{E}_0) \equiv I^{(\mathrm{loc})}(t,\ \mathcal{L}\,|\,\mathcal{E}_0) + I^{(\mathrm{rej})}(t,\ \mathcal{L}\,|\,\mathcal{E}_0)$ remains independent of $\overline{T}(|k_z|,\ \mathcal{L})$ or the randomness of a SL system, and it is solely determined by the nonequilibrium occupation function $\Delta n(k_z,\ t)$, which depends on interface-roughness parameters, DC-field strength, and temperature. In this way, randomness in the system only controls the ratio of forward to backward currents, while the interface roughness in this system determine their sum. Therefore, the interplay between weak-localization and interface-roughness effects on nonlinear electron transport within a SL is expected to be varied by different choices for intrinsic sample parameters, such as $s_1,\ s_2,\ N$, as well as $\Delta_0,\ \Lambda_0$, along with external conditions, e.g., $\rho_0,\ T$, and $\mathcal{E}_0$. This becomes the focus of our current study.

From Eqs. (3) and (11), we know that $\overline{T}(|k_z|,\ \mathcal{L}) \equiv 1$ if $s_1 = s_2$ is assumed. Therefore, the backward current $I^{(\mathrm{rej})}(t,\ \mathcal{L}\,|\,\mathcal{E}_0) \equiv 0$, and the total current is solely determined by the interface-roughness scattering of electrons, as displayed by the dotted curve in the upper-left panel of Fig. 5 and reported in our previous study [9]. For fixed $N = 50$, $s_1 = 0.01$, and $\mathcal{E}_0 = 0.5$ kV/cm, we find from the upper-left panel that the transient $I^{(\mathrm{loc})}(t,\ \mathcal{L}\,|\,\mathcal{E}_0)$ reaches its steady-state value at $t = 0.1$ ps for all cases considered, where steady-state $I^{(\mathrm{loc})}(t,\ \mathcal{L}\,|\,\mathcal{E}_0)$ becomes larger if s_2 approaches s_1 value and retains its value as small as possible. This reflects the randomness effect in the SL system on nonlinear electron transport. On the other hand, we also find from the lower-left panel of Fig. 5 that the steady-state $I^{(\mathrm{loc})}(t,\ \mathcal{L}\,|\,\mathcal{E}_0)$ increases with the DC-field strength $\mathcal{E}_0$ in a nonlinear way, which results from the interface-roughness effect on electron transport within a SL.

To explore further the randomness effect in the SL system, we fix s_1 as one of two random parameters, and we study the dependence of currents on another randomness parameter s_2. From Fig. 6 we find the steady-state forward current $I^{(\mathrm{loc})}(t,\ \mathcal{L}\,|\,\mathcal{E}_0)$, as well as the steady-state backward current $I^{(\mathrm{rej})}(t,\ \mathcal{L}\,|\,\mathcal{E}_0)$, as a function of s_2 (one of two randomness parameters) for fixed $s_1 = 0.01$, $N = 50$, $\mathcal{E}_0 = 0.5$ kV/cm, and $T = 4$ K. From this figure, we discover that $I^{(\mathrm{loc})}(t,\ \mathcal{L}\,|\,\mathcal{E}_0) < I^{(\mathrm{rej})}(t,\ \mathcal{L}\,|\,\mathcal{E}_0)$ is always maintained, which agrees with the observation in Fig. 3 that $\overline{T}(|k_z|,\ \mathcal{L}) < \overline{R}(|k_z|,\ \mathcal{L})$ for the occupied electronic states within the region of $|k_z| < \pi/2d$.

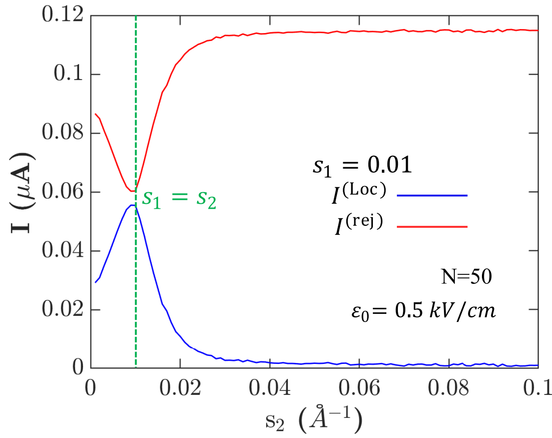

FIG. 6. Plots for forward $I^{(\text{loc})}(t,\ \mathcal{L}\,|\,\mathcal{E}_0)$ (blue) and backward $I^{(\text{rej})}(t,\ \mathcal{L}\,|\,\mathcal{E}_0)$ (red) steady-state electrical currents as a function of s_2 for $N = 50$, $\mathcal{E}_0 = \tilde{\mathcal{E}}_0$, $T = 4$ K, and $s_1 = 0.01$.

Moreover, $I^{(\text{loc})}(t,\ \mathcal{L}\,|\,\mathcal{E}_0)$ and $I^{(\text{rej})}(t,\ \mathcal{L}\,|\,\mathcal{E}_0)$ get their maximum and minimum values, respectively, as $s_2 = s_1 = 0.01$ is reached. Furthermore, $I^{(\text{loc})}(t,\ \mathcal{L}\,|\,\mathcal{E}_0)$ decays to zero as s_2 moves far away from $s_1 = 0.01$, which is accompanied by the rise of $I^{(\text{rej})}(t,\ \mathcal{L}\,|\,\mathcal{E}_0)$ to its full value $I_0(t,\ \mathcal{E}_0)$ (i.e., the dotted curve in the upper-left panel of Fig. 5) at the same time.

To demonstrate the interplay from interface-roughness scattering in the same system, we have fixed two random parameters s_1 and s_2 so as to investigate the DC-field dependence in steady-state forward $I^{(\text{loc})}(t,\ \mathcal{L}\,|\,\mathcal{E}_0)$ and backward $I^{(\text{rej})}(t,\ \mathcal{L}\,|\,\mathcal{E}_0)$ currents. After $s_1 = 0.01$, $s_2 = 0.05$, and $T = 4$ K are set, we display currents $I^{(\text{loc})}(t,\ \mathcal{L}\,|\,\mathcal{E}_0)$ and $I^{(\text{rej})}(t,\ \mathcal{L}\,|\,\mathcal{E}_0)$ as functions of field strength $\mathcal{E}_0$ in Fig. 7. It is clear from the left panel of Fig. 7 that, for a fixed value of $\mathcal{E}_0$, the magnitude of $I^{(\text{loc})}(t,\ \mathcal{L}\,|\,\mathcal{E}_0)$ decreases as the number of barrier layers N increases due to the enhanced randomness effect in the SL system. As expected, the opposite feature is observed for the backward current $I^{(\text{rej})}(t,\ \mathcal{L}\,|\,\mathcal{E}_0)$ presented in the right panel of Fig. 7 since the sum $I_0(t,\ \mathcal{E}_0) = I^{(\text{loc})}(t,\ \mathcal{L}\,|\,\mathcal{E}_0) + I^{(\text{rej})}(t,\ \mathcal{L}\,|\,\mathcal{E}_0)$ is always independent of N. Interestingly, as $\mathcal{E}_0$ becomes strong, the nonlinear dependence of currents on $\mathcal{E}_0$ shows up due to a full account of nonlinear electron transport beyond the usual linear-response theory, and it is a result of the exactly solved reduced Boltzmann transport equation in Eq. (13) for in-plane roughness scattering of electrons within a superlattice [9]. Here, the conductance, proportional to $\partial I^{(\text{loc})}(t,\ \mathcal{L}\,|\,\mathcal{E}_0)/\partial\mathcal{E}_0$, decreases with increasing field strength $\mathcal{E}_0$ and is fully caught by two plots for both $I^{(\text{loc})}(t,\ \mathcal{L}\,|\,\mathcal{E}_0)$ and $I^{(\text{rej})}(t,\ \mathcal{L}\,|\,\mathcal{E}_0)$ in this strong $\mathcal{E}_0$ limit. This unique N-dependent non-Ohmic behavior reflects clearly the interplay between in-plane roughness scattering of electrons and vertical scattering of electrons due to the existence of randomness in the SL system.

In fact, the contributions to the $\mathcal{E}_0$ field dependence of currents $I^{(\text{loc})}(t,\ \mathcal{L}\,|\,\mathcal{E}_0)$ and $I^{(\text{rej})}(t,\ \mathcal{L}\,|\,\mathcal{E}_0)$ come not only from the interface-roughness scattering, as discussed in Fig. 7, but also from the random scattering strengths distributed to periodically arranged finite number of barrier layers. In Fig. 8, we have fixed two random scattering-strength parameters $s_1 = 0.01$ and $s_2 = 0.005$ and displayed the dependence of currents $I^{(\text{loc})}(t,\ \mathcal{L}\,|\,\mathcal{E}_0)$ and $I^{(\text{rej})}(t,\ \mathcal{L}\,|\,\mathcal{E}_0)$ on the total number of barrier layers N for various strengths of a dc field. It is clear that the average transmission coefficient of electrons will rely on the total number of barrier layers if the randomness effect has been introduced to a SL system. As seen in Fig. 8, the increase of $\mathcal{E}_0$ values changes both forward current $I^{(\text{loc})}(t,\ \mathcal{L}\,|\,\mathcal{E}_0)$ as well as the total current $I_0(t,\ \mathcal{E}_0) = I^{(\text{loc})}(t,\ \mathcal{L}\,|\,\mathcal{E}_0) + I^{(\text{rej})}(t,\ \mathcal{L}\,|\,\mathcal{E}_0)$, as pointed out in the discussion at the beginning of Sec. IV B. Here, the variation of the N value corresponds to the change in the amount of randomness within the SL system. As anticipated, we find from Fig. 8 that the forward current $I^{(\text{loc})}(t,\ \mathcal{L}\,|\,\mathcal{E}_0)$ decreases with increasing N, but the backward current $I^{(\text{rej})}(t,\ \mathcal{L}\,|\,\mathcal{E}_0)$ increases with N, since the sum of these two should be a constant for a fixed value of $\mathcal{E}_0$, independent of the selected N value.

C. Dependence of localization length of electrons on sample length

The localization length $\xi_{\text{loc}}(\mathcal{L}\,|\,\mathcal{E}_0)$, which directly results from the existing randomness in a SL system, can be extracted from the calculated forward current $I^{(\text{loc})}(t,\ \mathcal{L}\,|\,\mathcal{E}_0)$ based on Eq. (12). Here, $\xi_{\text{loc}}(\mathcal{L}\,|\,\mathcal{E}_0)/\mathcal{L} = 1$ specifies a critical value $\mathcal{L}_c$ for the SL length beyond which $I^{(\text{loc})}(t,\ \mathcal{L}\,|\,\mathcal{E}_0)$ will start an exponential decay with respect to increasing $\mathcal{L}$. As

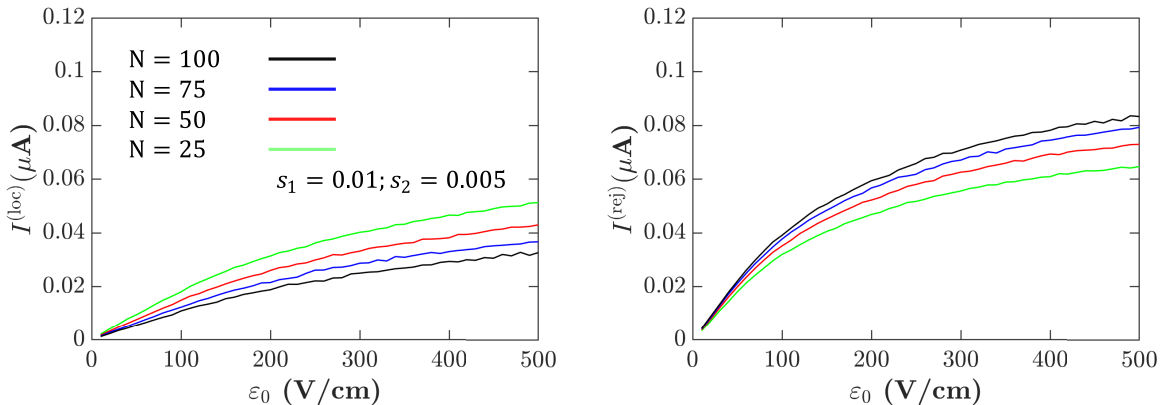

FIG. 7. Comparison of computed results for forward $I^{(\text{loc})}(t,\ \mathcal{L}\,|\,\mathcal{E}_0)$ (left) and backward $I^{(\text{rej})}(t,\ \mathcal{L}\,|\,\mathcal{E}_0)$ (right) steady-state electrical currents as a function of dc field $\mathcal{E}_0$ at $T = 4$ K for $s_1 = 0.01$, $s_2 = 0.005$, and various values of N.

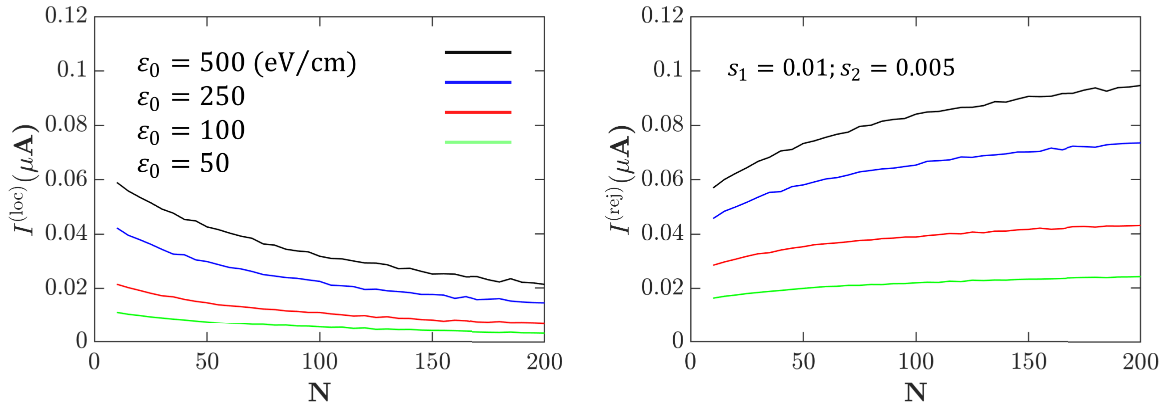

FIG. 8. Calculated forward $I^{(\mathrm{loc})}(t,\ \mathcal{L}\,|\,\mathcal{E}_0)$ (left) and backward $I^{(\mathrm{rej})}(t,\ \mathcal{L}\,|\,\mathcal{E}_0)$ (right) steady-state electrical currents at $T = 4$ K as a function of the number of barriers N for $s_1 = 0.01$, $s_2 = 0.005$, and various dc field strengths of $\mathcal{E}_0$.

seen in Fig. 9, the ratio $\xi_{\mathrm{loc}}(\mathcal{L}\,|\,\mathcal{E}_0)/\mathcal{L}$ decreases superlinearly with increasing N or randomness in the SL system, although $\mathcal{L} = (N + 1)\,d$ also increases linearly with N. Once the ratio $\xi_{\mathrm{loc}}(\mathcal{L}\,|\,\mathcal{E}_0)/\mathcal{L}$ drops below the dotted line for $\xi_{\mathrm{loc}}(\mathcal{L}\,|\,\mathcal{E}_0)/\mathcal{L} = 1$ in Fig. 9, this implies an occurrence of exponential decay with $\mathcal{L}$ for the forward current $I^{(\mathrm{loc})}(t,\ \mathcal{L}\,|\,\mathcal{E}_0)$. On the other hand, for fixed $s_1 = 0.01$ and N value, $\xi_{\mathrm{loc}}(\mathcal{L}\,|\,\mathcal{E}_0)/\mathcal{L}$ decreases as s_2 increases from 0.002 to 0.02 by an order of magnitude. For $s_2 = 0.015$ or 0.005 close to $s_1 = 0.01$, however, $\xi_{\mathrm{loc}}(\mathcal{L}\,|\,\mathcal{E}_0)/\mathcal{L}$ is enhanced relatively for fixed N due to reduced randomness in the system. Eventually, a sample satisfying $\xi_{\mathrm{loc}}(\mathcal{L}\,|\,\mathcal{E}_0)/\mathcal{L} < 1$ will be dominated by the weak-localization effect of electrons from vertical scattering, while the sample with $\xi_{\mathrm{loc}}(\mathcal{L}\,|\,\mathcal{E}_0)/\mathcal{L} > 1$ will be limited by the interface-roughness scattering effect of electrons from inplane scattering.

D. Controlling interplay of weak localization with interface-roughness scattering inside a superlattice

Finally, the unique field strength $\mathcal{E}_0$ dependence in $\xi_{\mathrm{loc}}(\mathcal{L}\,|\,\mathcal{E}_0)$ is compared in Fig. 10 for two temperatures $T = 4$ and 77 K with fixed $s_1 = 0.01$, $s_2 = 0.02$, and $N = 50$. Physically, the dependence of localization length $\xi_{\mathrm{loc}}(\mathcal{L}\,|\,\mathcal{E}_0)$ on $\mathcal{E}_0$ and T comes from its inclusion of the nonequilibrium occupation function $\Delta n(k_z, t)$ in the computation of $I^{(\mathrm{loc})}(t,\ \mathcal{L}\,|\,\mathcal{E}_0)$, which consists of all contributions from interface-roughness scattering as well as their dependence on external $\mathcal{E}_0$ and T through the reduced Boltzmann transport equation. When $T = 4$ K is assumed, we find from Fig. 10 that $\xi_{\mathrm{loc}}(\mathcal{L}\,|\,\mathcal{E}_0) < \mathcal{L}$, which implies that the forward current $I^{(\mathrm{loc})}(t,\ \mathcal{L}\,|\,\mathcal{E}_0)$ in this case is dominated by the weak-localization effect on electrons. As the temperature T is lifted up to 77 K, on the other hand, one gets $\xi_{\mathrm{loc}}(\mathcal{L}\,|\,\mathcal{E}_0) > \mathcal{L}$, indicating that $I^{(\mathrm{loc})}(t,\ \mathcal{L}\,|\,\mathcal{E}_0)$ in the system has already been controlled by interface-roughness scattering of electrons in this case instead of by the weak-localization effect at $T = 4$ K. Here, the observed temperature-dependent feature in Fig. 10 clearly demonstrates the capability for controlling nonlinear electron transport and the dynamics in interplay of weak localization in the z direction with interface roughness within the x-y plane inside a semiconductor superlattice.

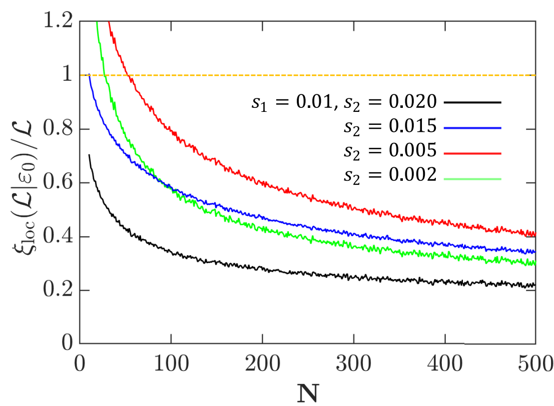

FIG. 9. Comparison of calculated localization lengths $\xi_{\mathrm{loc}}(\mathcal{L}\,|\,\mathcal{E}_0)$ at $T = 4$ K as a function of the total number of barrier layers N for $s_1 = 0.01$ and $\mathcal{E}_0 = \tilde{\mathcal{E}}_0$ with different values of s_2.

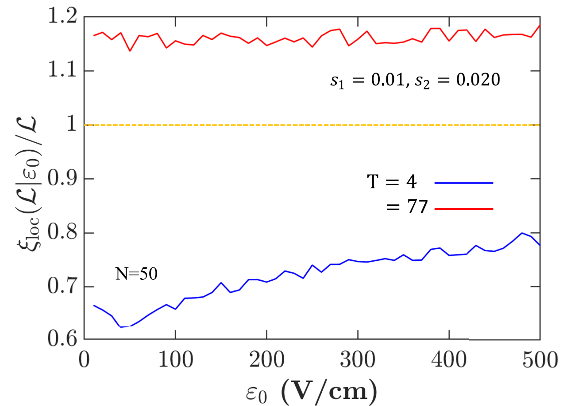

FIG. 10. Comparison for extracted localization lengths $\xi_{\mathrm{loc}}(\mathcal{L}\,|\,\mathcal{E}_0)$ at different temperatures $T = 4$ and 77 K as a function of DC-field strength $\mathcal{E}_0$ for $N = 50$, $s_1 = 0.01$, and $s_2 = 0.02$. Here, small but visible fluctuations in $\xi_{\mathrm{loc}}(\mathcal{L}\,|\,\mathcal{E}_0)$ result from minor uncertainty in performing its numerical computations associated with randomness average given by Eq. (11) in the text for a limited value of $N = 50$.

V. SUMMARY AND REMARKS

The localization effect on electronic transport was observed experimentally before [64] within a type-I GaAs-AlAs superlattice structure prepared by molecular-beam epitaxy. The measured differential conductance along the superlattice direction reveals a first gradually decreasing followed by a rapid dropping to negative values, then, at high fields, presenting an oscillatory behavior with respect to applied voltages. Such a phenomenon is believed to be connected to the formation and expansion of a high-field domain. Meanwhile, the voltage period of the oscillation provides the energy of the first-excited band. By theoretically treating perpendicular and transverse electron transports simultaneously, new calculations of low-temperature perpendicular and transverse electron mobilities in type-II InAs/GaSb superlattices were reported based on a relaxation-time approximation [46], indicating an important role played by the interface-roughness scattering in vertical transport. As a result, by making use of the calculated mobility curves, it allows one to extract the magnitude of a vertical mobility from measurements of the horizontal mobility [38]. Very recently, by applying effective scattering potentials, a self-consistent quantum-kinetic transport theory was proposed [9] for studying accurately both in-plane and out-of-plane scatterings of electrons within an infinitely-long GaAs/AlGaAs superlattice beyond the relaxation-time approximation. This rigorous theory reveals the unique nonlinear dependence of a vertical transport current on an applied dc field, temperature, and electron concentration. In this paper, we further generalize our previous theory [9] by considering an interplay between weak localization and interface-roughness scattering of vertical transport of electrons in a finite-length GaAs/AlGaAs superlattice structure accompanied by random barrier-height fluctuations in this system.

To highlight both in-plane scattering and barrier-fluctuation enabled localization mechanisms, as well as their interplay, we have chosen a relatively simple band structure, i.e., type-I superlattices for electrons only, instead of complex type-II superlattices utilized in experiments for both electrons and holes. As a result, a direct comparison of our numerical results with available magnetoexperimental data [38] turns out to be very difficult if not impossible. Moreover, the current study focuses on the dynamics of nonlinear transport of electrons in a strong-field regime, while the corresponding magnetoexperiments [38] are usually conducted within a weak-field regime and acquire a field-independent conductivity at the same time. Therefore, the parameters, such as ρ_0, T, $\bar{\mathcal{E}}_0$, N chosen in Table I, are only for a demonstration of interplay and unique dynamics behind the interface-roughness and fluctuated-barrier scatterings of electrons in superlattices but not for a specific comparison with available experimental measurements.

In summary, for electron transport within a superlattice, we have simultaneously explored two quite different physical aspects, including vertical scattering of electrons by randomly distributed barrier scattering strengths in a superlattice as well as by in-plane interface-roughness scattering of electrons for each barrier layer of the superlattice. For these two distinctive scattering mechanisms, we employ a single-electron transfer-matrix formalism to account for the existing randomness within a superlattice structure while applying the reduced Boltzmann transport equation to take into consideration of interface-roughness scattering of electrons within each barrier layer of the superlattice. Here, the group velocity of a single electron is replaced by a mean group velocity associated with an average transmission coefficient after the randomness has been introduced into this system. Furthermore, the electron transport current is obtained from another weighted average over the obtained mean group velocity with respect to a numerically computed nonequilibrium occupation function from the reduced Boltzmann transport equation for all available electronic states within the first Brillouin zone. For this case, the dynamical trapping of electrons occurs between different barrier layers within a superlattice and it can be included by using the single-electron transfer-matrix formalism. Meanwhile, electron scattering by interface roughness on each barrier layer is also taken into account by means of 1D effective interface-roughness scattering potentials employed in a reduced Boltzmann transport equation.

In this work, by including the interface-roughness scattering of electrons within each barrier layer of a superlattice, we reveal that the electrical current flowing through a superlattice depends on both the applied dc field strength $\mathcal{E}_0$ and temperature T, as seen in both Figs. 7 and 8, which further leads to a unique dependence of localization length on them in Fig. 10. Meanwhile, by including randomness in the barrier-scattering strengths of a superlattice, we find that the electrical current flowing through a superlattice also depends on the length of a superlattice, as presented in Figs. 7 and 8.

ACKNOWLEDGMENTS

D.H. would like to acknowledge the financial supports from the Air Force Office of Scientific Research (AFOSR). G.G. would like to acknowledge Grant No. FA9453-21-1-0046 from the Air Force Research Laboratory (AFRL). T.-N.D. would like to thank the NSTC of Taiwan for the support through Grant No. NSTC 111-2112-M-006 -010 - MY3. The views expressed are those of the authors and do not reflect the official guidance or position of the United States Government, the Department of Defense, or of the United States Air Force.

APPENDIX A: FULL BOLTZMANN TRANSPORT EQUATION FOR INTERFACE-ROUGHNESS SCATTERING OF ELECTRONS WITHIN A SUPERLATTICE

To study electrical current flowing through a superlattice (SL) structure under the influence of interface roughness, we apply our established nonlinear Boltzmann transport equation of electrons [55] in the form

$$\frac{d}{dt}f(\boldsymbol{k},t)=\left.\frac{\partial f(\boldsymbol{k},t)}{\partial t}\right|_{\mathrm{sc}}-\frac{\boldsymbol{F}_{\mathrm{DC}}(t)}{\hbar}\cdot\frac{\partial f(\boldsymbol{k},t)}{\partial \boldsymbol{k}},\qquad \text{(A1)}$$

where only one conduction miniband is taken into account in the electric-quantum limit for low electron volume density, low temperatures, and thin barrier layers in SL. In Eq. (A1), $f(\boldsymbol{k},t)$ is a nonequilibrium occupation function for miniband electrons in a SL, $\boldsymbol{k}=\{\boldsymbol{k}_\parallel,\,k_z\}$ is a 3D wave vector of

electrons, and $\boldsymbol{F}_{\rm DC}(t)$ stands for an applied dc electric-field force on electrons.

Here, we employ the Boltzmann-type scattering term for an energy-relaxation process in Eq. (A1), and we arrive at

$$\left.\frac{\partial f(\boldsymbol{k},t)}{\partial t}\right|_{\rm sc} = W_{\rm in}(\boldsymbol{k},t\,|\,f)[1-f(\boldsymbol{k},t)] - W_{\rm out}(\boldsymbol{k},t\,|\,f)\,f(\boldsymbol{k},t) \equiv W_{\rm in}(\boldsymbol{k},t\,|\,f) - \frac{f(\boldsymbol{k},t)}{\tau_{\rm E}(\boldsymbol{k})}, \tag{A2}$$

where $W_{\rm in}(\boldsymbol{k},t\,|\,f)$ and $W_{\rm out}(\boldsymbol{k},t\,|\,f)$ represent, respectively, the scattering-in and scattering-out rates for electrons with a wave vector $\boldsymbol{k}$, and they are calculated according to [55]

$$W_{\rm in}(\boldsymbol{k},t\,|\,f) = \frac{2\pi}{\hbar}\sum_{\mathbf{k}'}|V_{\rm ds}(\boldsymbol{k},\boldsymbol{k}')|^2\,f(\boldsymbol{k}',t)\,\delta(\varepsilon_{\mathbf{k}}-\varepsilon_{\mathbf{k}'})\,\Theta\,[\tilde{\varepsilon}_{\mathbf{k}}-E_z(k_z')], \tag{A3}$$

$$W_{\rm out}(\boldsymbol{k},t\,|\,f) = \frac{2\pi}{\hbar}\sum_{\mathbf{k}'}|V_{\rm ds}(\boldsymbol{k},\boldsymbol{k}')|^2[1-f(\boldsymbol{k}',t)]\,\delta(\varepsilon_{\mathbf{k}'}-\varepsilon_{\mathbf{k}})\,\Theta\,[\tilde{\varepsilon}_{\mathbf{k}}-E_z(k_z')], \tag{A4}$$

while the inverse energy-relaxation time introduced in Eq. (A2) is written as

$$\frac{1}{\tau_{\rm E}(\boldsymbol{k})} \equiv W_{\rm in}(\boldsymbol{k},t\,|\,f) + W_{\rm out}(\boldsymbol{k},t\,|\,f) = \frac{2\pi}{\hbar}\sum_{\mathbf{k}'}|V_{\rm ds}(\boldsymbol{k},\boldsymbol{k}')|^2\,\delta(\varepsilon_{\mathbf{k}}-\varepsilon_{\mathbf{k}'})\,\Theta[\tilde{\varepsilon}_{\mathbf{k}}-E_z(k_z')], \tag{A5}$$

which is independent of the occupation function $f(\boldsymbol{k},t)$. In Eqs. (A3) and (A4), $\varepsilon_{\mathbf{k}} \equiv \varepsilon_{\mathbf{k}_\parallel,k_z} = \hbar\Omega_0/2 + \hbar^2k_\parallel^2/2m^* + \mathcal{W}_0\sin^2(k_zd/2)$ stands for the kinetic energy of the lowest-miniband electrons in the SL with a period d, an isotropic in-plane effective mass m^*, a tight-binding miniband width $\mathcal{W}_0$, and a harmonic frequency Ω_0 from the quantum-well confinement, while $\tilde{\varepsilon}_{\mathbf{k}} = \varepsilon_{\mathbf{k}} - \hbar\Omega_0/2$. Moreover, $E_z(k_z) \equiv \mathcal{W}_0\sin^2(k_zd/2)$ and $\Theta(x)$ is a unity-step function [44,46]. Furthermore, the electron-electron and electron-phonon interactions have been ignored by assuming low doping densities and low temperatures. Meanwhile, the summations over $\boldsymbol{k}'$ in Eqs. (A3) and (A4) will exclude the term with $\boldsymbol{k}'=\boldsymbol{k}$. Furthermore, $|V_{\rm ds}(\boldsymbol{k},\boldsymbol{k}')|^2$ used in Eq. (A5) is the potential for dominant forward ($k_z'>0$) and secondly backward ($k_z'<0$) elastic scatterings [65] of miniband electrons by the presence of interface roughness within a SL structure, and it is given by [46]

$$|V_{\rm ds}(\boldsymbol{k},\boldsymbol{k}')|^2 = \frac{2\pi V_0^2\Delta_0^2\Lambda_0^2}{\mathcal{A}}\,e^{-q_\parallel^2\Lambda_0^2/4}\left|\phi_{k_z'}^{\rm SL}(a)\right|^2\left|\phi_{k_z}^{\rm SL}(a)\right|^2, \tag{A6}$$

where the site-correlation function for interface roughness is taken into account by means of a Gaussian model, roughness at both sides of a quantum well is also included, $\boldsymbol{q}=\boldsymbol{k}'-\boldsymbol{k}$ represents a transition wave vector for dominant forward/secondly backward electron scattering, as illustrated in Fig. 2, V_0 is the depth of a symmetrical quantum well for conduction electrons located at a two-edge quantum well at $z=\pm a$, Δ_0 and Λ_0 are the average amplitude and correlation length, respectively, for interface roughness, $\mathcal{A}$ is the cross-sectional area of SL, and $\phi_{k_z}^{\rm SL}(z)$ is the z-component of a full SL wave function $\Psi_{\mathbf{k}}^{\rm SL}(\boldsymbol{r}) = [\exp(i\boldsymbol{k}_\parallel\cdot\boldsymbol{r}_\parallel)/\sqrt{\mathcal{A}}\,]\,\phi_{k_z}^{\rm SL}(z)$. Different from the in-plane transport, the interface-roughness scattering for vertical transport of electrons is intrinsically a 3D process. Within the 1D tight-binding model, $\phi_{k_z}^{\rm SL}(z)$ takes the form [66]

$$\phi_{k_z}^{\rm SL}(z) = \frac{1}{\sqrt{N_0+1}}\sum_{j=0}^{N_0} e^{ik_zjd}\,\chi_0^{\rm QW}(z-jd) = \left[\phi_{-k_z}^{\rm SL}(z)\right]^*, \tag{A7}$$

where N_0+1 is the total number of quantum wells in a SL, and the individual quantum-well ground-state wave function takes the Gaussian form $|\chi_0^{\rm QW}(z)|^2 = (1/\sigma\sqrt{2\pi})\exp(-z^2/2\sigma^2)$ with $\sigma \lessapprox a < d/2$ for weak tunneling. In Eqs. (A3)–(A5), the umklapp-scattering process [67] for $|k_z'-k_z| > \pi/d$ could occur. To include this umklapp-scattering effect, we must replace k_z' by $k_z' \pm 2\pi/d$ to ensure that the new final scattering-state wave number $k_z' \pm 2\pi/d$ always remains within the first Brillouin zone $[-\pi/d,\ \pi/d]$.

In Eq. (A6), we have assumed that the dominant contribution for scattering of electrons in a SL is the interface roughness, while the other intrinsic electron-electron [68] and electron-phonon [69] scatterings are expected to be small for the case with a low doping density and low temperatures. To investigate the vertical transport of miniband electrons in a SL, we consider the total transient force $\boldsymbol{F}_{\rm DC}(t) = \mathcal{F}_{\rm DC}(t)\,\hat{\boldsymbol{e}}_z$ pointing towards the SL (or z) direction. Importantly, in order to cut down numerical computations, we will use an effective 1D occupation function $n(k_z,t)$ for nonequilibrium miniband electrons, written as

$$n(k_z,t) \equiv \frac{2}{n_{\rm qw}\mathcal{A}}\sum_{\mathbf{k}_\parallel} f(\boldsymbol{k},t) \approx \frac{1}{2\pi^2\rho_0 d}\int d^2\boldsymbol{k}_\parallel\,f(\{\boldsymbol{k}_\parallel,\ k_z\},\ t), \tag{A8}$$

where the spin degeneracy of electrons has already been included, the areal density $n_{\rm qw} \approx \rho_0 d$ for electrons in each quantum well is given by Eq. (23) since the total number of electrons in a SL remains as a constant, and ρ_0 is the volume density of doped electrons in a SL.

APPENDIX B: EFFECTIVE 1D INTERFACE-ROUGHNESS SCATTERING POTENTIALS

By means of Eqs. (18) and (19), we are able to calculate the effective 1D elastic-scattering potential $U_{\rm sc}(k_z,k_z')$, used by Eqs. (18) and (19), with the help of conservation of the total kinetic energy of electrons, yielding

$$
\begin{aligned}
U_{\rm sc}^{(\rm in)}(k_z,k_z') &= \frac{2}{n_{\rm qw}\mathcal{A}}\sum_{\mathbf{k}_\parallel,\mathbf{k}_\parallel'}|V_{\rm ds}(\boldsymbol{k},\boldsymbol{k}')|^2\,\delta(\varepsilon_{\mathbf{k}}-\varepsilon_{\mathbf{k}'})\,\Theta\big[\tilde{\varepsilon}_{\mathbf{k}_\parallel,k_z}-E_z(k_z')\big]\,[1-f_0[E_{xy}(k_\parallel)-\mu_0]]\,f_0[E_{xy}(k_\parallel')-\mu_0]\\
&\approx \frac{4\pi V_0^2\Delta_0^2\Lambda_0^2}{n_{\rm qw}}\left|\phi_{k_z'}^{\rm SL}(a)\right|^2\left|\phi_{k_z}^{\rm SL}(a)\right|^2\frac{1}{\mathcal{A}^2}\sum_{\mathbf{k}_\parallel}[1-f_0[E_{xy}(k_\parallel)-\mu_0]]\,\Theta\big[\tilde{\varepsilon}_{\mathbf{k}_\parallel,k_z}-E_z(k_z')\big]\\
&\quad\times\sum_{\mathbf{k}_\parallel'}\exp\left(-\frac{1}{4}\,|\boldsymbol{k}_\parallel-\boldsymbol{k}_\parallel'|^2\Lambda_0^2\right)\delta(\varepsilon_{\mathbf{k}_\parallel,k_z}-\varepsilon_{\mathbf{k}_\parallel',k_z'})\,f_0[E_{xy}(k_\parallel')-\mu_0]\\
&\approx \frac{V_0^2\Delta_0^2\Lambda_0^2}{2\pi^2 n_{\rm qw}}\left|\chi_0^{\rm QW}(a)\right|^4\int_0^\infty dk_\parallel\,k_\parallel\,[1-f_0[E_{xy}(k_\parallel)-\mu_0]]\,\Theta[\tilde{\varepsilon}_{\mathbf{k}_\parallel,k_z}-E_z(k_z')]\\
&\quad\times\int_0^\infty dk_\parallel'\,k_\parallel'\mathcal{L}_0(\varepsilon_{\mathbf{k}_\parallel,k_z}-\varepsilon_{\mathbf{k}_\parallel',k_z'},\,\Gamma_0)\int_0^{2\pi}d\theta_0\,\exp\left[-\frac{\mathcal{P}_0(k_\parallel,k_\parallel',\theta_0)\Lambda_0^2}{4}\right]f_0[E_{xy}(k_\parallel')-\mu_0],
\end{aligned}
\tag{B1}
$$

$$
\begin{aligned}
U_{\rm sc}^{(\rm out)}(k_z,k_z') &= \frac{2}{n_{\rm qw}\mathcal{A}}\sum_{\mathbf{k}_\parallel,\mathbf{k}_\parallel'}|V_{\rm ds}(\boldsymbol{k},\boldsymbol{k}')|^2\,\delta(\varepsilon_{\mathbf{k}}-\varepsilon_{\mathbf{k}'})\,\Theta\big[\tilde{\varepsilon}_{\mathbf{k}_\parallel,k_z}-E_z(k_z')\big]\,f_0[E_{xy}(k_\parallel)-\mu_0]\,[1-f_0[E_{xy}(k_\parallel')-\mu_0]]\\
&\approx \frac{4\pi V_0^2\Delta_0^2\Lambda_0^2}{n_{\rm qw}}\left|\phi_{k_z'}^{\rm SL}(a)\right|^2\left|\phi_{k_z}^{\rm SL}(a)\right|^2\frac{1}{\mathcal{A}^2}\sum_{\mathbf{k}_\parallel}f_0[E_{xy}(k_\parallel)-\mu_0]\,\Theta\big[\tilde{\varepsilon}_{\mathbf{k}_\parallel,k_z}-E_z(k_z')\big]\\
&\quad\times\sum_{\mathbf{k}_\parallel'}\exp\left(-\frac{1}{4}\,|\boldsymbol{k}_\parallel-\boldsymbol{k}_\parallel'|^2\Lambda_0^2\right)\delta\big(\varepsilon_{\mathbf{k}_\parallel,k_z}-\varepsilon_{\mathbf{k}_\parallel',k_z'}\big)\,[1-f_0[E_{xy}(k_\parallel')-\mu_0]]\\
&\approx \frac{V_0^2\Delta_0^2\Lambda_0^2}{2\pi^2 n_{\rm qw}}\left|\chi_0^{\rm QW}(a)\right|^4\int_0^\infty dk_\parallel\,k_\parallel\,f_0[E_{xy}(k_\parallel)-\mu_0]\,\Theta\big[\tilde{\varepsilon}_{\mathbf{k}_\parallel,k_z}-E_z(k_z')\big]\\
&\quad\times\int_0^\infty dk_\parallel'\,k_\parallel'\mathcal{L}_0\big(\varepsilon_{\mathbf{k}_\parallel,k_z}-\varepsilon_{\mathbf{k}_\parallel',k_z'},\,\Gamma_0\big)\int_0^{2\pi}d\theta_0\,\exp\left[-\frac{\mathcal{P}_0(k_\parallel,k_\parallel',\theta_0)\Lambda_0^2}{4}\right][1-f_0[E_{xy}(k_\parallel')-\mu_0]].
\end{aligned}
\tag{B2}
$$

In Eqs. (B1) and (B2), $\mathcal{P}_0(k_\parallel,k_\parallel',\theta_0)=k_\parallel^2+k_\parallel'^2-2k_\parallel k_\parallel'\cos\theta_0\geqslant 0$, and θ_0 is the angle between two in-plane wave vectors $\boldsymbol{k}_\parallel$ and $\boldsymbol{k}_\parallel'$, $U_{\rm sc}^{(\rm out)}(k_z,k_z')=U_{\rm sc}^{(\rm out)}(k_z,-k_z')=U_{\rm sc}^{(\rm out)}(-k_z,k_z')$ for randomized in-plane scattering, and $|\chi_0^{\rm QW}(a)|=|\chi_0^{\rm QW}(-a)|$ for a symmetrical quantum well. In Eqs. (B1) and (B2), $U_{\rm sc}(k_z,k_z')\geqslant 0$, $\mathcal{L}_0(a,b)=b/[\pi(a^2+b^2)]$ is a Lorentz-shape function, Γ_0 (much smaller than $\mathcal{W}_0$) is the inverse lifetime of conduction electrons, $\tilde{\varepsilon}_{\mathbf{k}_\parallel,k_z}\equiv\varepsilon_{\mathbf{k}_\parallel,k_z}-\hbar\Omega_0/2=E_{xy}(k_\parallel)-\hbar\Omega_0/2+\mathcal{W}_0\sin^2(k_zd/2)\equiv\tilde{E}_{xy}(k_\parallel)+E_z(k_z)$ is the total-energy dispersion for miniband electrons with nearest-neighbor coupling in a 1D tight-binding model, and the variable in Lorentz-shape function is given explicitly by $\tilde{\varepsilon}_{\mathbf{k}_\parallel,k_z}-\tilde{\varepsilon}_{\mathbf{k}_\parallel',k_z'}=[E_z(k_z)-E_z(k_z')]+[\tilde{E}_{xy}(k_\parallel)-\tilde{E}_{xy}(k_\parallel')]$. Importantly, only the total kinetic energy of scattering electrons in Eqs. (B1) and (B2) is required to be conserved but not the individual ones in either the longitudinal or transverse direction. Furthermore, we will employ the relations $k_\parallel dk_\parallel=(m^*/\hbar^2)\,d\tilde{E}_{xy}(k_\parallel)$ and $dk_z'=(2/\mathcal{W}_0d)\,dE_z(k_z')/\sqrt{1-\{1-(2/\mathcal{W}_0)[E_z(k_z')+\Gamma_0]\}^2}$ for the calculations included in Eqs. (B1) and (B2), where $\tilde{E}_{xy}(k_\parallel)=\hbar^2k_\parallel^2/2m^*$ and $E_z(k_z')=\mathcal{W}_0\,\sin^2(k_z'd/2)$. From Eqs. (B1) and (B2), we know that such a 3D scattering process, as illustrated in Fig. 2, can be viewed effectively as a quasi-1D process after an average with respect to in-plane scatterings of electrons has been performed.

Here, we emphasize that the obtained reduced 1D scattering potentials $U_{\rm sc}^{(\rm in)}(k_z,k_z')$ and $U_{\rm sc}^{(\rm out)}(k_z,k_z')$ in Eqs. (B1) and (B2), which are associated with initial-/final-state electron wave numbers k_z and k_z' in a quasi-1D superlattice system, actually correspond to an inelastic-scattering process for electrons in a superlattice, although its original form with an anisotropic energy dispersion remains as an elastic-scattering process for electrons in a 3D bulk system.

[1] C. P. Umbach, S. Washburn, R. B. Laibowits, and A. Webb, Magnetoresistance of small, quasi-one-dimensional, normal-metal rings and lines, Phys. Rev. B **30**, 4048 (1984).

[2] D. Y. Sharvin and Y. V. Sharvin, Magnetic-flux quantization in a cylindrical film of a normal metal, Pis'ma Zh. Eksp. Teor. Fiz. **34**, 285 (1981) [JETP Lett. **34**, 272 (1981)].

[3] R. A. Webb, S. Washburn, C. P. Umbach, and R. B. Laibowitz, Observation of $\hbar/e$ Aharonov-Bohm oscillations in normal-metal rings, Phys. Rev. Lett. **54**, 2696 (1985).

[4] B. L. Al'tshuler, Fluctuations in the extrinsic conductivity of disordered conductors, JETP Lett. **41**, 648 (1985).

[5] P. A. Lee and A. D. Stone, Universal conductance fluctuations in metals, universal conductance fluctuations in metals, Phys. Rev. Lett. **55**, 1622 (1985).

[6] S. Datta, M. R. Melloch, S. Bandyopadhyay, and S. Lundstrom, Proposed structure for large quantum interference effects, Appl. Phys. Lett. **48**, 487 (1986).

[7] S. Datta, *Extended Abstracts of the 20th International Conference on Solid State Devices and Materials* (Business Center for Academic Societies Japan, Tokyo, Japan, 1988), p. 491.

[8] M. Yamamoto and K. Hohkawa, *Extended Abstracts of the 20th International Conference on Solid State Devices and Materials* (Business Center for Academic Societies Japan, Tokyo, Japan, 1988), p. 495.

[9] P.-H. Shih, D. H. Huang, G. Gumbs, T.-N. Do, C. P. Morath, and T. Maestas, Effects of interface-roughness scattering on nonlinear electron transport in a superlattice based on exact solution of generalized Boltzmann transport equation, Phys. Rev. B **108**, 165304 (2023).

[10] A. R. Goñi, A. Pinczuk, J. S. Weiner, J. M. Calleja, B. S. Dennis, L. N. Pfeiffer, and K. W. West, One-dimensional plasmon dispersion and dispersionless intersubband excitations in GaAs quantum wires, Phys. Rev. Lett. **67**, 3298 (1991).

[11] R. Landauer, Spatial variation of currents and fields due to localized scatterers in metallic conduction, IBM J. Res. Dev. **1**, 223 (1957); D. S. Fisher and P. A. Lee, Relation between conductivity and transmission matrix, Phys. Rev. B **23**, 6851 (1981).

[12] D. Shechtman, I. Blech, D. Gratias, and J. W. Chan, Metallic phase with long-range orientational order and no translational symmetry, Phys. Rev. Lett. **53**, 1951 (1984).

[13] Y. Avishai and D. Berend, Transmission through a one-dimensional Fibonacci sequence of δ-function potentials, Phys. Rev. B **41**, 5492 (1990); M. Kolá and M. K. Ali, Generalized Fibonacci superlattices, dynamical trace maps, and magnetic excitations, *ibid.* **39**, 426 (1989); M. Kohmoto, L. P. Kadanoff, and C. Tang, Localization problem in one dimension: Mapping and escape, Phys. Rev. Lett. **50**, 1870 (1983); Q. Niu and F. Nori, Renormalization-group study of one-dimensional quasiperiodic systems, *ibid.* **57**, 2057 (1986); Z. Cheng, R. Savit, and R. Merlin, Structure and electronic properties of Thue-Morse lattices, Phys. Rev. B **37**, 4375 (1988).

[14] B. Simon, Almost periodic Schrödinger operators: A Review, Adv. Appl. Math. **3**, 463 (1982); J. B. Sokoloff, Unusual band structure, wave functions and electrical conductance in crystals with incommensurate periodic potentials, Phys. Rep. **126**, 189 (1985).

[15] D. H. Huang, J. P. Peng, and S. X. Zhou, Intrasubband and intersubband plasmons in a semi-infinite Fibonacci HgTe/CdTe superlattice, Phys. Rev. B **40**, 7754 (1989).

[16] D. H. Huang, G. Gumbs, and M. Kolář, Localization in a one-dimensional Thue-Morse chain, Phys. Rev. B **46**, 11479 (1992).

[17] D. H. Huang and G. Gumbs, Finite-size effect on neutron polarization in a one-dimensional quasiperiodic magnetic lattice, Solid State Commun. **84**, 1061 (1992).

[18] G. Gumbs, G. S. Dubey, A. Salman, B. S. Mahmoud, and D. Huang, Statistical and transport properties of quasiperiodic layered structures: Thue-Morse and Fibonacci, Phys. Rev. B **52**, 210 (1995).

[19] D. H. Huang, G. Gumbs, Y. Zhao, and G. W. Auner, Optical-phonon transport and localization in periodic and Fibonacci polar-semiconductor superlattices, Phys. Lett. A **200**, 459 (1995).

[20] Y. Zhao, D. H. Huang, and R. Shen, C omparative study of one-dimensional photonic bandgap structures using multilayer nonlinear thin films, J. Nonlin. Opt. Phys. Mater. **04**, 1 (1995).

[21] G. F. Lorusso, V. Capozzi, J. L. Staehli, C. Flesia, D. Martin, and P. Favia, Absorption spectra of $GaAs/Al_xGa_{1-x}As$ random superlattices at 2K, Phys. Rev. B **53**, 1018 (1996).

[22] R. Farchioni and G. Grosso, Electric-field effect on the transmittivity of aperiodic Kronig-Penney crystals, Phys. Rev. B **56**, 1981 (1997).

[23] D. H. Huang, A. Singh, and D. A. Cardimona, Effects of structural disorders on sequential tunneling in multiple quantum wells, Phys. Lett. A **259**, 488 (1999).

[24] A. Rogalski and P. Martyniuk, InAs/GaInSb superlattices as a promising material system for third generation infrared detectors, Infr. Phys. Technol. **48**, 39 (2006); A. Rogalski, J. Antoszewski, and L. Faraone, Third-generation infrared photodetector arrays, J. Appl. Phys. **105**, 091101 (2009).

[25] Q. K. Yang, F. Fuchs, J. Schmitz, and W. Pletschen, Investigation of trap-assisted tunneling current in InAs/(GaIn)Sb superlattice long-wavelength photodiodes, Appl. Phys. Lett. **81**, 4757 (2002).

[26] R. Rehm, M. Walther, F. Fuchs, J. Schmitz, and J. H. Fleissner, Investigation of trap-assisted tunneling current in InAs/(GaIn)Sb superlattice long-wavelength photodiodes, Appl. Phys. Lett. **86**, 173501 (2005).

[27] B.-M. Nguyen, D. Hoffman, E. K.-W. Huang, P.-Y. Delaunay, and M. Razeghi, Background limited long wavelength infrared type-II InAs/GaSb superlattice photodiodes operating at 110 K, Appl. Phys. Lett. **93**, 123502 (2008); S. A. Pour, E. K. Huang, G. Chen, A. Haddani, B.-M. Nguyen, and M. Razeghi, High operating temperature midwave infrared photodiodes and focal plane arrays based on type-II InAs/GaSb superlattices, *ibid.* **98**, 143501 (2011).

[28] A. Hood, M. Razeghi, E. H. Aifer, and G. J. Brown, On the performance and surface passivation of type II InAs/GaSb superlattice photodiodes for the very-long-wavelength infrared, Appl. Phys. Lett. **87**, 151113 (2005).

[29] H. J. Haugan, F. Szmulowicz, K. Mahalingam, G. J. Brown, S. R. Munshi, and B. Ullrich, On the performance and surface passivation of type II InAs/GaSb superlattice photodiodes for the very-long-wavelength infrared, Appl. Phys. Lett. **87**, 261106 (2005).

[30] F. Szmulowicz, H. J. Haugan, G. J. Brown, K. Mahalingam, B. Ullrich, S. R. Munshi, and L. Grazulis, Interfaces as design tools for short-period InAs/GaSb type-II superlattices for mid-infrared detectors, Opto-Electron. Rev. **14**, 69 (2006).

[31] E. Plis, J. B. Rodriguez, G. Balakrishnan, Y. D. Sharma, H. S. Kim, T. Rotter, and S. Krishna, Mid-infrared InAs/GaSb strained layer superlattice detectors with nBn design grown on a GaAs substrate, Semicond. Sci. Technol. **25**, 085010 (2010).

[32] W. W. Bewley, J. R. Lindle, C. S. Kim, M. Kim, C. L. Canedy, I. Vurgaftman, and J. R. Meyer, Lifetimes and Auger coefficients in type-II W interband cascade lasers, Appl. Phys. Lett. **93**, 041118 (2008).

[33] J. B. Rodriguez, C. Cervera, and P. Christol, A type-II superlattice period with a modified InAs to GaSb thickness ratio for midwavelength infrared photodiode performance improvement, Appl. Phys. Lett. **97**, 251113 (2010).

[34] N. Yoon, C. J. Reyner, G. Ariyawansa, J. M. Duran, J. E. Scheihing, J. Mabon, and D. Wasserman, Modified electron beam induced current technique for In(Ga)As/InAsSb superlattice infrared detectors, J. Appl. Phys. **122**, 074503 (2017).

[35] F. Aristone, J.-C. Portal, J. F. Palmier, and J. C. Harmand, Shubnikov-de Haas-like oscillations in the vertical transport of semiconductor superlattices, Braz. J. Phys. **29**, 375 (1999); A. Sibille, J. F. Palmier, H. Wang, and F. Mollot, Observation of Esaki-Tsu negative differential velocity in GaAs/AlAs superlattices, Phys. Rev. Lett. **64**, 52 (1990); F. Aristone, P. Gassot, J. F. Palmier, D. K. Maude, B. Goutiers, J. L. Gauffier, J. C. Portal, and G. Mollot, Probing the interface fluctuations in semiconductor superlattices using a magneto-transport technique, Superlattices Microstruct. **15**, 225 (1994).

[36] G. A. Umana-Membreno, H. Kala, J. Antoszewski, J. M. Dell, L. Faraone, B. Klein, G. Gautam, M. N. Kutty, E. Plis, S. Krishna and L. Faraone, Vertical transport in InAs/GaSb type-II strained layer superlattices for infrared focal plane array applications, Proc. SPIE **8012**, 80120Y (2011).

[37] L. Bürkle, F. Fuchs, R. Kiefer, W. Pletschen, R. E. Sah, and J. Schmits, Electrical Characterization of InAs/(GaIn) Sb infrared superlattice photodiodes for the 8 to 12 μm range, MRS Online Proceedings Library **607**, 75 (1999).

[38] L. K. Casias, C. P. Morath, E. H. Steenbergen, G. A. Umana-Membreno, P. T. Webster, J. V. Logan, J. K. Kim, G. Balakrishnan, L. Faraone, and S. Krishna, Vertical carrier transport in strain-balanced InAs/InAsSb type-II superlattice material, Appl. Phys. Lett. **116**, 182109 (2020).

[39] R. W. Prange and T. W. Nee, Quantum spectroscopy of the low-field oscillations in the surface impedance, Phys. Rev. **168**, 779 (1968); H. Sakaki, T. Noda, K. Hirakawa, M. Tanaka, and T. Matsusue, Interface roughness scattering in GaAs/AlAs quantum wells, Appl. Phys. Lett. **51**, 1934 (1987); T. Noda, M. Tanaka, and H. Sakaki, Correlation length of interface roughness and its enhancement in molecular beam epitaxy grown GaAs/AlAs quantum wells studied by mobility measurement, *ibid.* **57**, 1651 (1990); U. Penner, H. Rücker, and I. N. Yassievich, Theory of interface roughness scattering in quantum wells, Semicond. Sci. Technol. **13**, 709 (1998); N. Balkan, R. Gupta, M. Cankurtaran, H. Celik, A. Bayrakli, E. Tiras, and M. CÂ¸ Arikan, Well-width dependence of interface roughness scattering in $GaAs/Ga_{1-x}Al_xAs$ quantum wells, Superlattice Microstruct. **22**, 263 (1997); R. Nag, S. Mukyopadhyay, and M. Das, Interface roughness scattering-limited electron mobility in AlAs/GaAs and $Ga_{0.5}In_{0.5}P$/GaAs wells, J. Appl. Phys. **86**, 459 (1999); J. M. Li, J. J. Wu, X. X. Han, Y. W. Lu, X. L. Liu, Q. S. Zhu, and Z. G. Wang, A model for scattering due to interface roughness in finite quantum wells, Semicond. Sci. Technol. **20**, 1207 (2005); B. R. Nag, Interface roughness scattering limited mobility in AlAs/GaAs, $Al_{0.3}Ga_{0.7}As$/GaAs and $Ga_{0.5}In_{0.5}P$/GaAs quantum wells, *ibid.* **19**, 162 (2004); A. Gold, Interface-roughness parameters in InAs quantum wells determined from mobility, J. Appl. Phys. **103**, 043718 (2008).

[40] F. Szmulowicz and G. J. Brown, Calculation of the vertical and horizontal electron mobilities in InAs/GaSb superlattices, Appl. Phys. Lett. **98**, 182105 (2011); F. Szmulowicz and G. J. Brown, Vertical transport in InAs/GaSb superlattices: model results and relation to in-plane transport, Proc. SPIE **7945**, 79451U (2011).

[41] S. Mori and T. Ando, Electronic properties of a semiconductor superlattice II. Low temperature mobility perpendicular to the superlattice, J. Phys. Soc. Jpn. **48**, 865 (1980).

[42] I. Dharssi and P. N. Butcher, The effect of phonon confinement on perpendicular electron transport in a GaAs/GaAlAs superlattice, J. Phys.: Condens. Matter **2**, 119 (1990).

[43] J. Q. You, L. Zhang, and Q. B. Yang, Longitudinal magnetotransport in long-period semiconductor superlattices, Phys. Rev. B **55**, 15757 (1997); G. J. Warren and P. N. Butcher, A mobility calculation for a GaAs/GaAlAs superlattice, Semicond. Sci. Technol. **1**, 133 (1986).

[44] G. Etemadi and J. F. Palmier, Effect of interface roughness on non-linear vertical transport in GaAs/AlAs superlattices, Solid State Commun. **86**, 739 (1993).

[45] J. R. Meyer, D. J. Arnold, C. A. Hoffman, F. J. Bartoli, and L. R. Ram-Mohan, Electron and hole in-plane mobilities in HgTe-CdTe superlattices, Phys. Rev. B **46**, 4139 (1992); C. A. Hoffman, J. R. Meyer, E. R. Youngdale, F. J. Bartoli, R. H. Miles, and L. R. Ram-Mohan, Electron transport in $InAs/Ga_{1-x}In_xSb$ superlattices, Solid-State Electron. **37**, 1203 (1994); Y. A. Pusep, G. C. Gozzo, and R. R. LaPierre, Interface roughness in short-period InGaAs/InP superlattices, Appl. Phys. Lett. **93**, 242104 (2008); T. V. Chandrasekhar Rao, J. Antoszewski, L. Faraone, J. B. Rodriguez, E. Plis, and S. Krishna, Characterization of carriers in GaSb/InAs superlattice grown on conductive GaSb substrate, *ibid.* **92**, 012121 (2008); C. Cervera, J. B. Rodrigue, J. P. Perez, H. Ait-Kaci, R. Chaghi, L. Konczewicz, S. Contreras, and P. Christol, Unambiguous determination of carrier concentration and mobility for InAs/GaSb superlattice photodiode optimization, J. Appl. Phys. **106**, 033709 (2009).

[46] F. Szmulowicz, H. J. Haugan, S. Elhamri, and G. J. Brown, Calculation of vertical and horizontal mobilities in InAs/GaSb superlattices, Phys. Rev. B **84**, 155307 (2011).

[47] L. Esaki and R. Tsu, Superlattice and negative differential conductivity in semiconductors, IBM J. Res. Dev. **14**, 61 (1970).

[48] H.-B. Lin, H. Zhong, N. Karpowicz, Y. Chen, and X.-C. Zhang, Terahertz spectroscopy and imaging for defense and security applications, Proc. IEEE **95**, 1514 (2007).

[49] D. Suqing, W. Zhang, and X.-G. Zhao, Current response of two-band superlattices at finite temperatures, Phys. Rev. B **62**, 9943 (2000).

[50] Z.-G. Wang, D. Suqing, and X.-G. Zhao, Photon-assisted transport and dynamical localization of semiconductor superlattices under a dc bichromatic electric field, Phys. Rev. B **69**, 035305 (2004).

[51] D. H. Dunlap and V. M. Kenkre, Dynamic localization of a charged particle moving under the influence of an electric field, Phys. Rev. B **34**, 3625 (1986).

[52] V. I. Puller, N. J. M. Horing, Lev G. Mourokh, and A. Yu. Smirnov, Wave packet dynamics in a semiconductor superlattice, Phys. Lett. A **281**, 70 (2001).

[53] M. M. Dignam and C. M. de Sterke, Conditions for dynamic localization in generalized ac electric fields, Phys. Rev. Lett. **88**, 046806 (2002).

[54] M. J. Zhu, X.-G. Zhao, and Q. Niu, Manipulation of band electrons with a rectangular-wave electric field, J. Phys.: Condens. Matter **11**, 4527 (1999).

[55] J. R. Gulley and D. H. Huang, Self-consistent quantum-kinetic theory for interplay between pulsed-laser excitation and

nonlinear carrier transport in a quantum-wire array, Opt. Expr. **27**, 17154 (2019).

[56] A. Chomette, B. Deveaud, A. Regreny, and G. Bastard, Observation of carrier localization in intentionally disordered Gaas/Gaalas superlattices, Phys. Rev. Lett. **57**, 1464 (1986).

[57] B. V. Olson, J. F. Klem, E. A. Kadlec, J. K. Kim, M. D. Goldflam, S. D. Hawkins, A. Tauke-Pedretti, W. T. Coon, T. R. Fortune, E. A. Shaner, and M. E. Flatté, Vertical hole transport and carrier localization in $InAs/InAs_{1-x}Sb_x$ Type-II superlattice heterojunction bipolar transistors, Phys. Rev. Appl. **7**, 024016 (2017).

[58] S.-J. Xiong, Theoretical investigation of current-noise characteristics in finite semiconductor superlattice with correlated thickness randomness, J. Appl. Phys. **78**, 6079 (1995).

[59] B. F. Levine, Quantum-well infrared photodetectors, J. Appl. Phys. **74**, R1 (1993).

[60] D. H. Huang, S. K. Lyo, and G. Gumbs, Bloch oscillation, dynamical localization, and optical probing of electron gases in quantum-dot superlattices in high electric fields, Phys. Rev. B **79**, 155308 (2009).

[61] G. Gumbs and D. H. Huang, *Properties of Interacting Low-Dimensional Systems* (Wiley, Weinheim, 2011).

[62] S. Datta, *Electronic Transport in Mesoscopic Systems* (Cambridge University Press, Cambridge, UK, 1997).

[63] E. P. Wigner, On the quantum correction for thermodynamic equilibrium, Phys. Rev. **40**, 749 (1932).

[64] L. Esaki and L. L. Chang, New transport phenomenon in a semiconductor superlattice, Phys. Rev. Lett. **33**, 495 (1974).

[65] S. K. Lyo and D. H. Huang, Multisublevel magnetoquantum conductance in single and coupled double quantum wires, Phys. Rev. B **64**, 115320 (2001).

[66] Y. Zhu, D. H. Huang, and S. Feng, Tunneling plasmon excitations in quasi-zero-dimensional superlattices composed of quantum dots, Phys. Rev. B **40**, 3169 (1989.

[67] S. Ono, Thermalization in simple metals: Role of electron-phonon and phonon-phonon scattering, Phys. Rev. B **97**, 054310 (2018).

[68] S. K. Lyo and D. H. Huang, Effect of electron-electron scattering on the conductance of a quantum wire studied with the Boltzmann transport equation, Phys. Rev. B **73**, 205336 (2006).

[69] S. K. Lyo and D. H. Huang, Temperature-dependent magnetoconductance in quantum wires: Effect of phonon scattering, Phys. Rev. B **68**, 115317 (2003).